B2. MARGINS-funded Research Nuggets

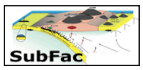

Subduction Factory

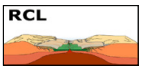

Rupturing Continental Lithosphere

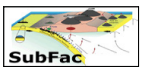

Source-to-Sink

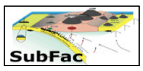

Seismogenic Zone Experiment

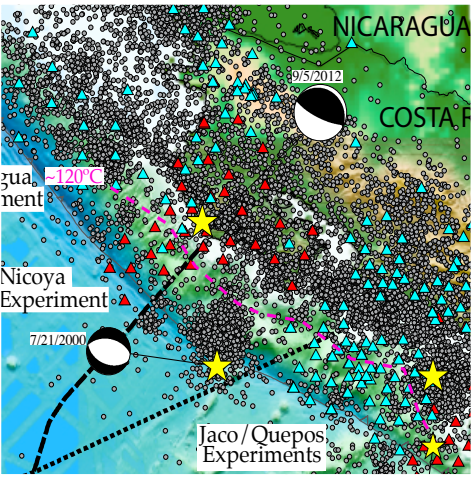

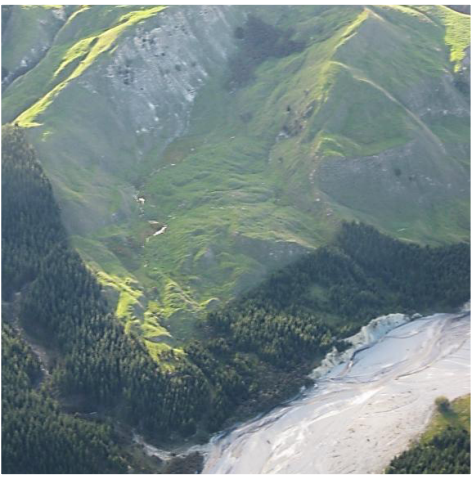

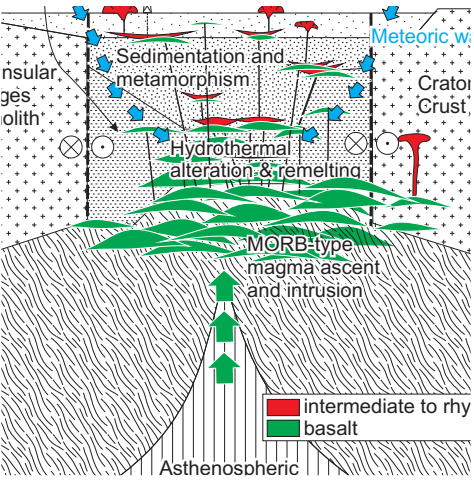

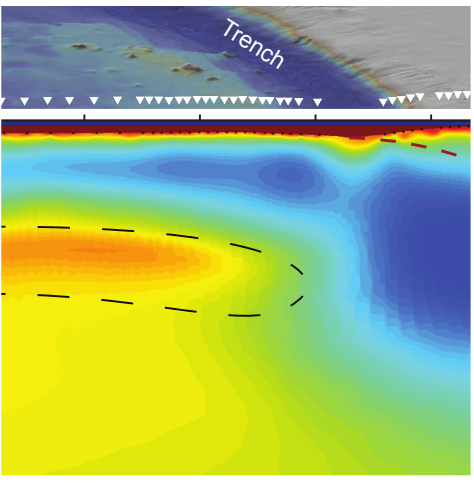

MARGINS

MARGINS Nuggets

Imaging 3D Seismic Velocity and Attenuation Heterogeneity Along the Seismogenic Zone of Costa Rica and Nicaragua, MARGINS Program

Heather R. DeShon*, Melissa M. Moore-Driskell, Shishay T. Bisrat, Center for Earthquake Research and Information, University of Memphis. *now at Southern Methodist University

The Nicaragua/Costa Rica segment of the Middle America subduction zone exhibits seismogenic zone characteristics that are strongly dependent on plate structure, temperature, and fluid-related processes. Because some rock properties, such as fluid content, have a greater effect on attenuation than velocity, combining 3D attenuation and seismic velocity models is useful to improve our interpretation of the complex processes and material properties along the subduction fault. Velocity and attenuation models calculated as part of this study were aimed at characterizing lateral and down-dip variability along the megathrust of this erosive margin. The study integrates data from onshore/offshore seismic networks along the Osa and Nicoya Peninsulas, Costa Rica, collected as part of CRSEIZE (NSF, PIs. S. Schwartz/L. Dorman) and along central Costa Rica and Nicaragua collected as part of the SFB 574 program (PIs. E. Flueh/W. Rabbel) [Moore-Driskell et al., 2013] (Figure 1a). The integrated data was used to calculate continuous along-strike compressional (Vp) and shear (Vs) velocity, Vp/Vs [Driskell, 2012] and compressional attenuation (Qp) models [Bisrat, 2013]. Some velocity images also included TUCAN data (NSF, PIs. K. Fisher and G. Abers). Comparative analysis of variations in attenuation, seismic velocities, seismicity rates, and coseismic slip along the margin yields valuable insight into determining the controlling factors in earthquake nucleation.

High-resolution Vp, Vs, and Vp/Vs images were computed for Nicaragua/Costa Rica using double-difference local earthquake tomography [Driskell, 2012; Moore-Driskell et al., in preparation]. Waveform cross-correlation significantly improved differential time data used in the tomographic inversions [Moore-Driskell et al., 2013]. We find that the up-dip limit of seismogenic zone microseismicity varies along-strike, broadly corresponds to the 150° C isotherm and is located closer to the trench in Nicaragua, which is consistent with plate coupling models. All seismogenic zone seismicity resides in a low Vp band that parallels the top of the high velocity subducting slab. This low Vp band thins and weakens from north to south and may reflect changes in pore fluid pressure along the plate interface. In areas of well-resolved Vp/Vs, we image a transition from low Vp/Vs to high Vp/Vs at the downdip edge of seismogenic zone seismicity. Comparisons of interseismic activity across the margin with subduction tremor, slow slip, geodetic data and mainshock slip patterns suggest that tremor and/or slow slip may be a better proxy for the limit of rupture during major earthquakes.

Attenuation images were computed for the Nicoya Peninsula segment of the seismogenic zone corresponding to the 2012 M7.6 Nicoya Peninsula underthrusting earthquake [Bisrat, 2013] (Figure 1b). Path attenuation (t*) measurements derived from P-wave spectra were used to calculate a 3D Qp model using local earthquake tomography methods. The 2012 mainshock rupture corresponds to reduced Vp (Figure 1b) and reduced Vp/Vs within the Nicoya seismogenic zone. The corresponding attenuation indicates that the strongly coupled parts of the megathrust are characterized by low attenuation (higher Qp) (Figure 1b). In contrast, the upper crust of the overriding plate, fluid-rich part of the crust and the tip of the mantle wedge exhibit high attenuation values (low Qp). Low frequency earthquakes reported along the seismogenic zone tend to occur in high attenuation regions near the Moho discontinuity.

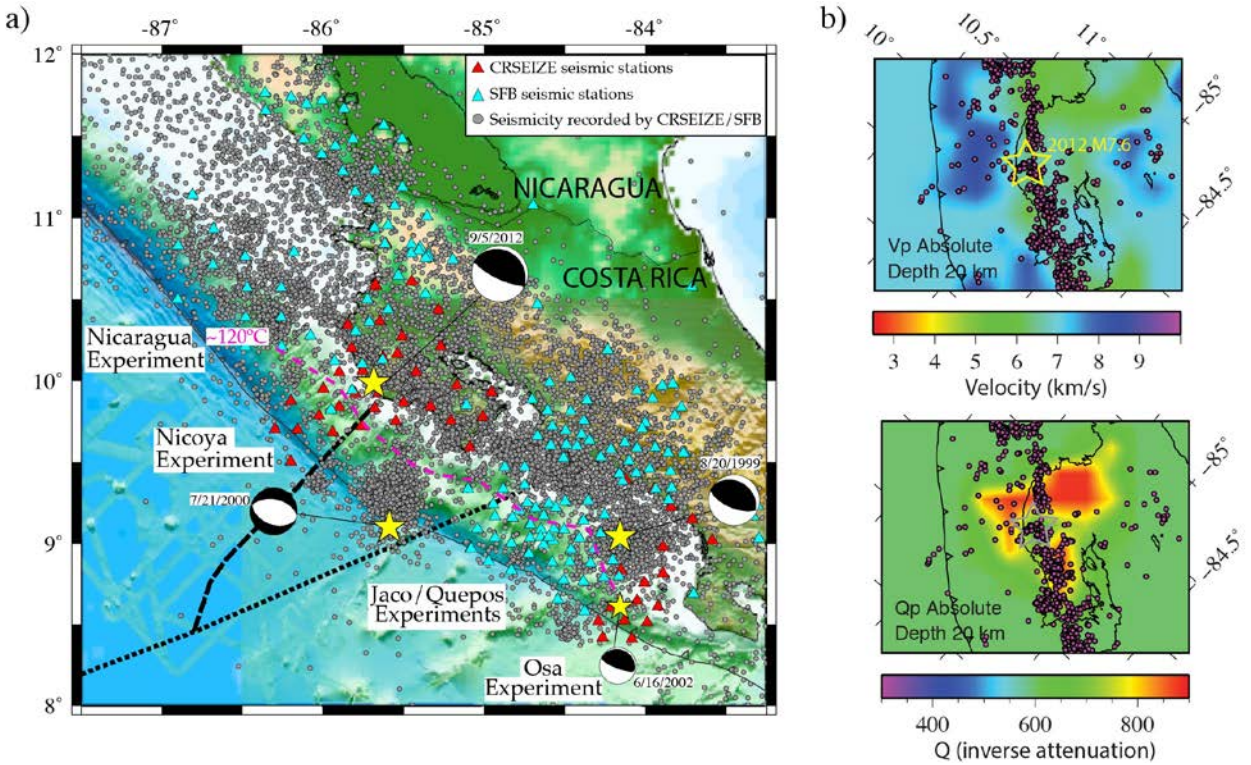

Figure 1: a) Overview of the Costa Rica-Nicaragua margin. Highlighted are the temporary on- and offshore passive seismic networks and associated earthquake catalogs used in this study. b) Compressional velocity and attenuation models for the Nicoya Peninsula seismogenic zone plotted at 20 km depth, which includes the seismogenic zone. The star shows the approximate rupture area of the 2012 M7.6 Nicoya underthrusting earthquake.

Publications cited:

Bisrat, S. (2013), Chapter 4: Investigating the 3-D attenuation structure of the Nicoya Peninsula, Costa Rica, using local earthquake tomography, in *Three Dimensional Attenuation and High Resolution Earthquake Location: Applications to the New Madrid Seismic Zone and Costa Rica Seismogenic Zone*, PhD Dissertation, Univ. of Memphis.

Driskell, M. (2012), *3D Double Difference Tomography of the Middle America Subduction Zone Beneath Nicaragua and Costa Rica*, PhD Dissertation, Univ. of Memphis.

Moore-Driskell, M., H.R. DeShon, W. Rabbel, 3D double difference velocity tomography of the Middle America subduction zone beneath Costa Rica and Nicaragua, in preparation/revisions.

Moore-Driskell, M., H.R. DeShon, W. Rabbel, M.M. Thorwart, Y. Dzierma (2013), Integration of arrival time datasets for consistent quality control: A case study of amphibious experiments along the Middle America Trench, *Bulletin of the Seismological Society of America*, 103(5), doi: 10.1785/0120120274, 2752-2766.

Collaborative Research: The oxidation state of Mariana arc magmas and its relationship to subduction volatile and mass cycling

Katherine A. Kelley & Maryjo Brounce, University of Rhode Island, Narragansett, RI
Elizabeth Cottrell, Smithsonian Institution, Washington, DC

Awarded under MARGINS, this project aimed to examine natural glasses from along and across the Mariana arc/trough system, in conjunction with analog piston-cylinder experiments equilibrating basalt with arc-relevant upper mantle phase assemblages at known fO_2, with the goals of (1) testing magmatic $Fe^{3+}/\sum Fe$ ratios against alternative proxies of both melt and mantle oxidation state (2) evaluating the role of magmatic processes, volatiles, and slab-derived components in influencing oxidation state, and (3) modeling the effects of the subduction cycle on the long-term evolution of redox conditions in the earth's interior.

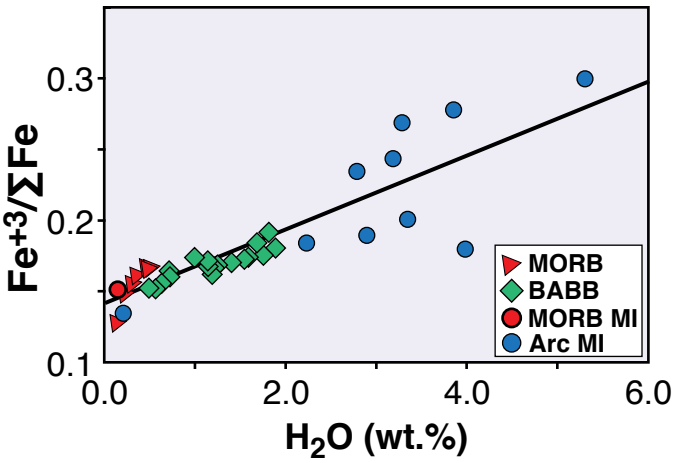

From Kelley & Cottrell (2009). Plot of measured H_2O concentrations vs. $Fe^{3+}/\sum Fe$ determined by μ-XANES for MORB and BABB glasses, and olivine-hosted melt inclusions (MI) from MORB and global arc volcanoes. $Fe^{3+}/\sum Fe$ in MI have been corrected for post-entrapment olivine crystallization or outward Fe^{2+} diffusion to place the melt compositions in equilibrium with the host olivine. Data for H_2O are published FTIR data from the literature or are FTIR or SIMS data from this study. Symbols exceed the size of the error bars in $Fe^{3+}/\sum Fe$ (±0.0045 [1σ]). The solid line is a least-squares linear regression through all of the data, with equation y=0.026x+0.14 (r^2=0.72). Using MORB and BABB data only, linear regression gives y=0.018+0.14 (r^2=0.65).

• Arc basalts globally, and within the Marianas, are more oxidized than MORB, and oxidation correlates with slab tracers (e.g., H_2O, Ba/La ratio). Oxidation is coincident with the arrival of slab tracers in the arc mantle during subduction initiation.

• Redox conditions of the MORB mantle are comparatively uniform, although subtle variations in MORB oxidation correlate with isotopic ratios sensitive to mantle source composition.

Publications:

Cottrell, E., K. A. Kelley, A. T. Lanzirotti, and R. A. Fischer (2009), High-precision determination of iron oxidation state in silicate glasses using XANES, Chem. Geol., 268, 167-179, doi:10.1016/j.chemgeo.2009.08.008.

Kelley, K. A., and E. Cottrell (2009), Water and the oxidation state of subduction zone magmas, Science, 325, 605-607, doi:10.1126/science.1174156.

Cottrell, E., and K. A. Kelley (2011), The oxidation state of Fe in MORB glasses and the oxygen fugacity of the upper mantle, Earth Planet. Sci. Lett., 305(3-4), 270-282, doi:10.1016/j.epsl.2011.03.014.

Kelley, K. A., and E. Cottrell (2012), The influence of magmatic differentiation on the oxidation state of Fe in a basaltic arc magma, Earth Planet. Sci. Lett., 329-330, 109-121, doi:10.1016/j.epsl.2012.02.010.

Cottrell, E., and K. A. Kelley (2013), Redox Heterogeneity in Mid-Ocean Ridge Basalts as a Function of Mantle Source, Science, 340(6138), 1314-1317, doi:10.1126/science.1233299.

Brounce, M. N., K. A. Kelley, and E. Cottrell (2014), Variations in $Fe^{3+}/\sum Fe$ of Mariana Arc Basalts and Mantle Wedge fO_2, J. Pet., 55(12), 2513-2536, doi:10.1093/petrology/egu065.

Brounce, M. N., K. A. Kelley, E. Cottrell, and M. K. Reagan (2015; in press), Temporal evolution of mantle wedge oxygen fugacity during subduction initiation, Geology, doi:10.1130/G36742.1.

THIN PARTIAL MELT CHANNEL DISCOVERED AT THE LITHOSPHERE-ASTHENOSPHERE BOUNDARY WITH MARINE MAGNETOTELLURIC DATA

Samer Naif, Kerry Key, Steven Constable, Rob L. Evans

Global seismic observations sporadically detect a sharp lithosphere-asthenosphere boundary (LAB) that is typically less than 30 km thick beneath oceanic plates. The strength of the anomalies cannot be explained by temperature alone. Either hydration or partial melt mechanisms have been invoked, with some debate as to which is the appropriate model. In 2010, we carried out the largest marine electromagnetic (EM) experiment across a subduction zone to date. A total of 54 broadband ocean-bottom EM instruments were deployed at the Middle America Trench offshore of Nicaragua. Our analysis of the magnetotelluric (MT) data led us to make an unexpected discovery. We imaged a low resistivity channel at 45-70 km depths beneath the 24 million-year-old (Ma) Cocos oceanic plate that extends seaward of the outer rise (Naif et al., 2013). The resistivity signature of the channel requires enough water that partial melting would ensue, whereby a small fraction of partial melt (1-2%) must be present. The extent of the channel suggests that deeper asthenospheric melts may rise buoyantly and become trapped at the base of the lithosphere. Numerical modeling studies support the possibility of melt accumulation at the LAB (Havlin et al., 2013). Alternatively, the melt may have been emplaced near the ridge-axis and persists in the melt stability zone defined by the solidus of damp peridotite. The channel is moderately anisotropic. This suggests warm and young regions of oceanic plates with a sharp LAB contain partial melt channels of low viscosity that are sheared along the direction of plate motion, acting as a lubricant to plate motion. We interpret the channel's confined depth extent as evidence that the lithosphere is decoupled from the deeper asthenosphere. A more recent active-source seismic experiment in New Zealand also detected a thin anomalous channel at the LAB that was interpreted as a zone of partial melt beneath a much older (120 Ma) oceanic plate (Stern et al., 2015). Therefore, it is possible that such channels are a common feature near subduction zones.

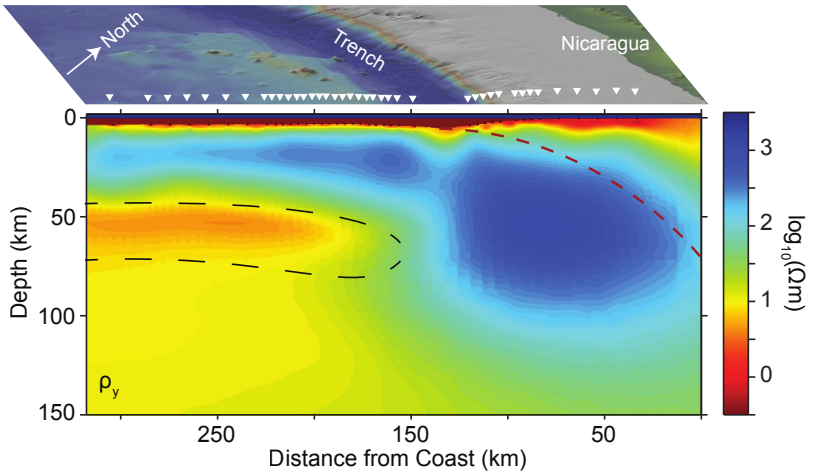

Anisotropic 2D inversion of the MT data. Blue and red colors denote resistive and conductive regions. The dashed black line marks the conductive channel at the LAB that we interpret as a zone of partial melt.

Citations:

Naif, S., K. Key, S. Constable, and R. L. Evans (2013), Melt-rich channel observed at the lithosphere–asthenosphere boundary, Nature, 495(7441), 356–359.

Havlin, C., E. M. Parmentier, G. Hirth (2013), Dike propagation driven by melt accumulation at the lithosphere-asthenosphere boundary, Earth Planet. Sci. Lett.. 376, 20¬–28.

Stern, T. A., S. A. Henrys, D. Okaya, J. N. Louie, M. K. Savage, S. Lamb, H. Sato, R. Sutherland, and T. Iwasaki (2015), A seismic reflection image for the base of a tectonic plate, Nature, 518(7537), 85–88.

IMAGING FLUID PATHWAYS AND MAPPING POROSITY ACROSS THE MIDDLE AMERICA TRENCH

Samer Naif[1], Kerry Key[1], Steven Constable[1], Rob L. Evans[2]

[1]Scripps Institution of Oceanography [2]Woods Hole Oceanographic Institution

In April 2010, we performed the first (and still only) marine controlled-source electromagnetic (CSEM) experiment of a subduction zone. The survey included over 800 line-km of transmitter tow across 44 broadband seafloor EM instruments, spanning the trench-outer rise and forearc slope of the Cocos and Caribbean tectonic plates. The CSEM data were first modeled in 1D and detected a significant reduction in the electrical resistivity coincident with the onset of bending faults in the outer rise (Key et al., 2012). The electrical anisotropy of the seafloor was also determined by deploying two sets of orthogonal long-wire EM instruments; the abyssal plain is relatively isotropic whereas the outer rise seafloor has a strong anisotropy parallel with the fabric of bending faults. Taken together, the CSEM data confirmed that reactivated normal faults enhance the porosity of oceanic crust, corroborating active-source seismic observations in the region (e.g., van Avendonk et al., 2011).

Subsequently, we modeled the data with newly developed 2D numerical tools (Key, 2012). The results showcase the powerful capacity of the CSEM method to image hydrogeologic processes and map porosity. We detected sub-vertical conductive channels along bending faults, which yield a two-fold increase in the pore water content of the intrusive crust and significantly raise the magnitude of H_2O entering the margin (Naif et al., accepted). The laterally varying structure suggests a heterogeneously hydrated oceanic plate, which has been shown to have a significant impact on the pattern and magnitude of H_2O fluxes in the mantle wedge (Wada et al., 2012). We also imaged a conductive channel at the plate interface caused by subducted sediments. We were able to utilize the resistivity signature to provide the first geophysical constraints of porosity at the plate interface. Our estimates match well with laboratory compaction studies from nearby borehole drilling samples (Spinelli et al., 2006; Lauer & Saffer, 2012).

Citations:

Key, K., S. Constable, T. Matsuno, R. L. Evans, and D. Myer (2012), Electromagnetic detection of plate hydration due to bending faults at the Middle America Trench, *Earth Planet. Sci. Lett.*, *351*, 45–53.

Key, K. (2012), Marine EM inversion using unstructured grids: a 2D parallel adaptive finite element algorithm, in *SEG Technical Program Expanded Abstracts 2012*, pp. 1–5, Society of Exploration Geophysicists.

Lauer, R. M., and D. M. Saffer (2012), Fluid budgets of subduction zone forearcs: the contribution of splay faults, *Geophys. Res. Lett.*, *39*, L13604.

Naif, S., K. Key, S. Constable, R. L. Evans (2015), Water-rich bending faults at the Middle America Trench, *Geochem. Geophys. Geosys., accepted.*

Spinelli, G. A., D. M. Saffer, and M. B. Underwood (2006), Hydrogeologic responses to three-dimensional temperature variability, Costa Rica subduction margin, *J. Geophys. Res.*, *111*, B04403.

van Avendonk, H. J. A., W. S. Holbrook, D. Lizarralde, and P. Denyer (2011), Structure and serpentinization of the subducting Cocos plate offshore Nicaragua and Costa Rica, *Geochem. Geophys. Geosys.,* 12, Q06009.

Wada, I., M. D. Behn, and A. M. Shaw (2012), Effects of heterogeneous hydration in the incoming plate, slab rehydration, and mantle wedge hydration on slab-derived H2O flux in subduction zones, *Earth Planet. Sci. Lett.*, 353-354, 60–71.

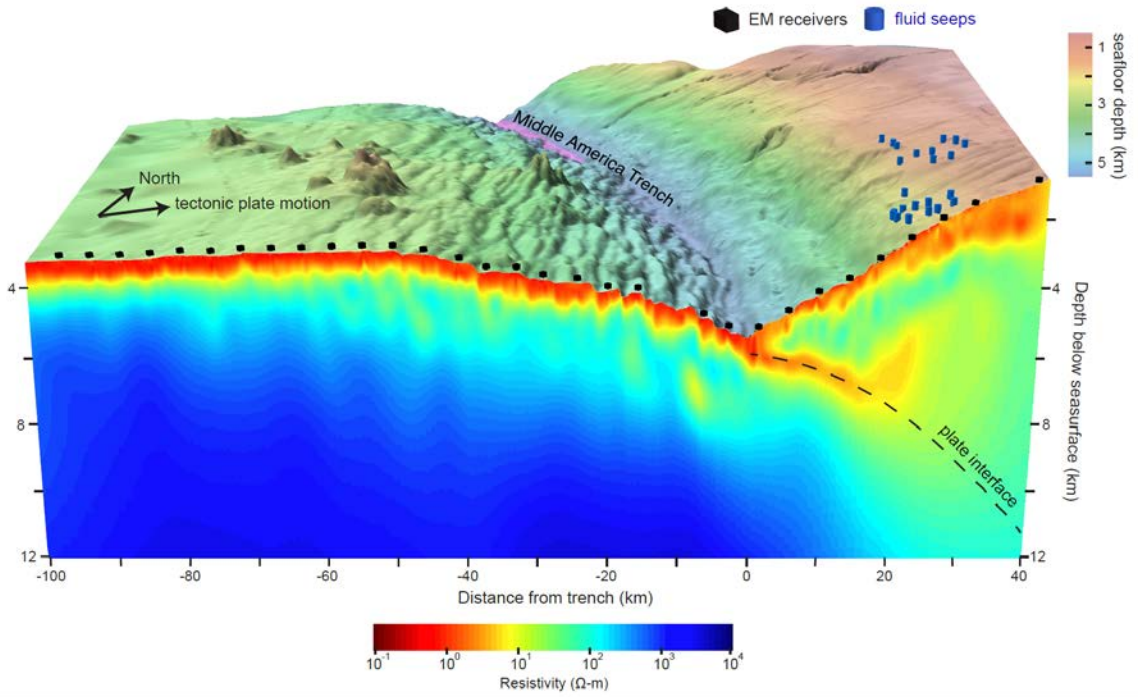

The electrical structure of the incoming Cocos plate from nonlinear inversion of deep-towed CSEM data. The vertical cross-section shows the sub-seafloor electrical resistivity structure and the stitched upper panel shows seafloor bathymetry. The black cubes show the location of EM receivers. The region of the seafloor marked by steeply dipping relief correlates with sub-vertical conductive channels, which we interpret as evidence for the migration of seawater along bending faults. The channel of low resistivity beneath the forearc – congruent with the geometry of the plate interface – is caused by subducted sediments.

NSF grant #EAR-0840862: Mariana Forearc Geology and Early Arc Volcanism

M.K. Reagan, W.C. McClelland, & D.W. Peate; University of Iowa

Grant funds were used to investigate the genesis of crust associated with subduction initiation and early arc development in the western Pacific. We analyzed igneous rocks from the Izu-Bonin-Mariana (IBM) fore-arc collected during HOV Shinkai 6500 diving for a broad spectrum of compositional traits. By integrating our results and those of IBM fore-arc islands and drill sites, we developed a comprehensive model of IBM fore-arc development. Before the proposal was submitted, Reagan and collaborators from the US and Japan conducted six Shinkai 6500 dives in the Mariana fore-arc southeast of Guam during one cruise of the R/V Yokosuka. Another dive cruise in the same area took place shortly after the proposal was submitted. The success of these two cruises led JAMSTEC to fund two additional cruises in 2009 (PI Osamu Ishizuka) and 2010 (PI Yasuhiko Ohara), the first in the Bonin fore-arc trenchward of the Ogasawara Ridge, the second in the same general region as the first two cruises. In total, 26 dives were undertaken, which collected a broad suite of basement lithologies related to the nascent Bonin and Mariana arcs. The funding from this grant was used for travel, sample processing and analysis, and to publish results from all four cruises.

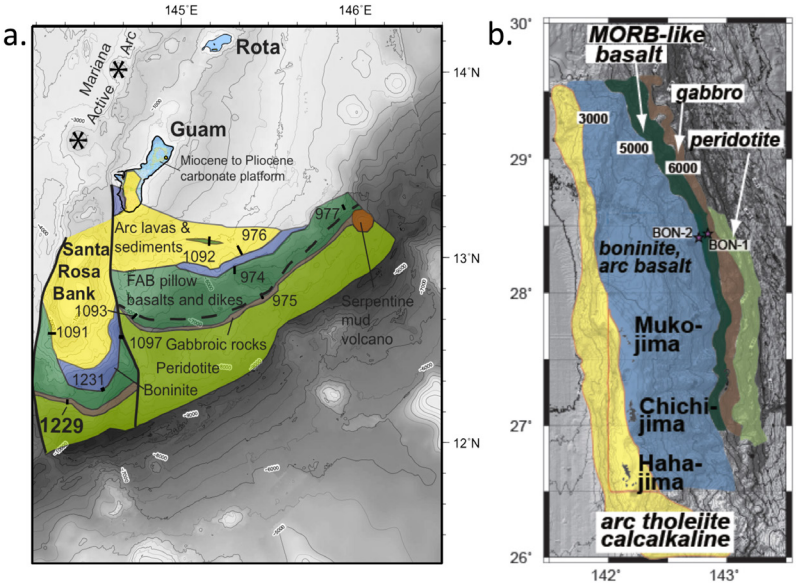

Figure 1. Geological sketch maps of the (a) Mariana fore-arc (Reagan et al., 2013) and (b) Bonin fore-arc (after Ishizuka et al. 2011). Numbers and associated tracks in (a) are for Shinkai 6500 dives. Bon-1 and Bon-2 in (b) are the approximate locations for two of the drill sites for IODP Exp. 352.

We discovered that the most abundant igneous rocks in the Mariana and Bonin fore-arcs are MORB-like basalts and related intrusive rocks. These basalts were part of a stratigraphic sequence like those commonly found in ophiolites (i.e. from trench to fore-arc high: depleted peridotite, gabbro, dolerite, basalt, boninite and arc lavas; Reagan et al., 2010; Ishizuka et al. 2011; Reagan et al., 2013; Fig. 1). The term "fore-arc basalt (FAB)" was coined for the basal basalts (Reagan et al., 2010) to illustrate that their compositions differ in detail from mid-ocean ridge and back-arc basin basalts, and that they have a separate tectonic origin. Although FAB have light–depleted rare earth element patterns similar to those of basalts from other oceanic extensional tectonic environments, FAB have lower Yb/V and Ti/V, and are therefore unusually large degree melts of strongly depleted mantle sources (Reagan et al., 2010). Radiogenic isotopic compositions indicate that, like other IBM magmas, FAB were derived from mantle similar to the source of Indian Ocean MORB (Ishizuka et al., 2011), although some Mariana FAB have Pb isotopic compositions consistent with a weak influence of subducted

Pacific crust (Reagan et al., 2010). Our $^{40}Ar/^{39}Ar$ and U-Pb zircon ages for FAB and associated intrusive rocks are identical within error in the Mariana and Bonin fore-arcs, suggesting that FAB magmatism occurred along the length of the subduction zone from ~51 to 52 Ma, which preceded boninite eruption by 2–4 My and normal arc volcanism by 7-8 My (Ishizuka et al., 2011; Reagan et al., 2013). Lavas from DSDP Sites 458 and 459 were found to have compositions and ages marking the transition from FAB to boninite.

Based on these data, we concluded that FAB were the first lavas to erupt when the Pacific Plate began sinking beneath the Philippine Plate at 52-51 Ma. The magmas were generated by mantle decompression during near-trench spreading with little or no mass transfer from the subducting plate. Boninites were generated later when the residual, highly depleted mantle melted at shallow levels after fluxing by a water-rich fluid derived from the sinking Pacific Plate. Our results support the concept that ophiolites with boninite overlying basalt were generated during subduction initiation events (Reagan et al., 2010; Stern et al., 2012).

Two ancillary hypotheses based on our research were presented in Reagan et al. (2013) and Turner et al. (2014). The former hypothesized that the widespread volcanism associated the subduction initiation event in the western Pacific contributed to the Early Eocene Climate Optimum hothouse period. The latter illustrated the similarity in igneous stratigraphic relationships between the IBM fore-arc and the potentially Hadean Nuvvuagittuq supracrustal belt in Quebec, and suggested that transient subduction could have started that far back in Earth's history. Turner et al. (2014) further speculated that RNA-based life could have started in a fore-arc setting because of the stabilizing affect that subduction-related, B-rich waters could have had on RNA.

One unexpected result of the diving was the discovery of the "Shinkai Seep Field," a *Vesicomyid* clam community associated with a serpentinite-hosted hydrothermal vent system in the southern Mariana forearc (Ohara et al., 2012). We documented the presences of a diverse community of organisms ultimately based on chemosynthesis of H_2 and CH_4 by microorganisms in alkaline fluids that originated in the subducting slab.

The final paper associated with this grant documented the evolution of mantle fO_2 between FAB and boninite. It illustrates that oxidation commences upon subduction initiation and matures rapidly in mantle wedge magma sources (Brounce et al., in press).

Finally, the published work associated with this grant laid the foundation for IODP Expeditions 351 and 352, which occurred during the summer of 2014. A primary objective of Expedition 351 was identifying and modeling subduction initiation by drilling the early Cenozoic sedimentary sequence in the Bonin rear arc (http://publications.iodp.org/scientific_prospectus /351/index.html). Expedition 352 successfully recovered a high-fidelity record of FAB to boninite volcanism in the Bonin fore-arc (http://publications.iodp.org/preliminary_report/352/).

References

Brounce, M., Kelley, K.A., Cottrell, E., and Reagan, M.K., in press, Temporal evolution of mantle wedge oxygen fugacity during subduction initiation. Geology.

Ishizuka, O., Tani, K., Reagan, M.K., 2014, Izu-Bonin-Mariana fore-arc crust as a modern ophiolite analogue. Elements, v. 10, p. 115-120. doi:10.2113/gselements.10.2.115

Turner, S., Rushmer, T., Reagan, M., Moyen, J-F., 2014, Heading down early on? Start of subduction on Earth. Geology, v. 42, p. 139-142. doi:10.1130/G34886.1

Reagan, M.K., McClelland, W.C. Girard, G., Goff, K.R., Peate, D.W., Ohara, Y., & Stern, R.J., 2013, The geology of the southern Mariana fore-arc crust: implications for the scale of Eocene volcanism in the western Pacific. Earth and Planetary Science Letters, v. 380, p. 41-51. doi:10.1016/j.epsl.2013.08.013

Stern, R.J., Reagan, M.K., Ishizuka, O., Ohara, Y., and Whattam, S., 2012, To Understand Subduction Initiation, Study Forearc Crust; To Understand Forearc Crust, Study Ophiolites. Lithosphere v. 4 p. 469-483. doi:10.1130/L183.1

Ohara,Y., Reagan, M.K., Fujikura, K., Watanabe., H., Michibayashi, K., Ishii, T., Stern, R.J., Pujana, J.I., Martinez, F., Girard, G., Ribeiro, J., Brounce, M., Naoaki K., and Kino, M., 2012, A serpentinite-hosted ecosystem in the Southern Mariana Forearc. Proceedings of the National Academy of Sciences. PNAS, v. 109 p. 2831–2835. doi:10.1073/pnas.1112005109

Ishizuka, O., Tani, K., Reagan, M.K., Kanayama, K., Umino, S., Harigane, Y., Sakamoto, I., Miyajima, Y., Yuasa, M., Dunkley, D.J., 2011, The timescales of subduction initiation and subsequent evolution of an oceanic island arc. Earth and Planetary Science Letters, v. 306 p. 229-240. doi:10.1016/j.epsl.2011.04.006

Reagan, M.K., Ishizuka, O., Stern, R.J., Kelley, K.A., Ohara, Y., Blichert-Toft, J., Bloomer, S.H., Cash, J., Fryer, P., Hanan, B., Hickey-Vargas, R., Ishii, T., Kimura, J-I., Peate, D.W., Rowe, M.C., and Woods, M., 2010, Fore-arc basalts and subduction initiation in the Izu-Bonin-Mariana system. Geochemistry Geophysics Geosystems. v. 11, doi: 10.1029/2009GC002871, 17 pp.

The temporal evolution of the Mariana Island Arc: the marine tephra record

MARGINS EAR 08-40848
Starting date: 15 April 2009

Susanne M. Straub[1], Jon D. Woodhead[2], Richard Arculus[3]

[1]*Lamont Doherty Earth Observatory at the Columbia University*
[2]*Melbourne School of Earth Sciences, University of Melbourne, Australia*
[3]*Research School of Earth Sciences, The Australian National University, Canberra*

The geochemical evolution of volcanic arcs provides insights into the growth of arc andesitic crust through time. Tephras recovered by deep-sea drilling from fore-arc to back-arc locations across the Mariana Volcanic Arc record the last 34 Myr of the system's evolution with high temporal precision and an average inter-tephra layer interval of ~1 Myr. Fresh tephra particles (glass, scoria, pumice) were used to obtain major and trace elements and Sr-Nd-Pb-Hf isotopic composition(Straub et al., 2015). Results are presented in Figure 1 together with a similar tephra record from the adjacent Izu Bonin arc that evolved contemporaneously (Straub et al., 2009; 2010). Key findings can be summarized as follows:

- Both arcs display steady trends of crust-forming major elements through time (exemplified by $Si_{4.0}$) that are decoupled from trace element and isotope variations. This suggests steady formation of arc andesitic crust since arc initiation.
- Sr-Nd-Pb isotope ratios confirm that the well-known divergence of source-sensitive trace element through time (Lee et al., 1995; Bryant et al., 1999) is linked to changes in the slab input, and not to intra-crustal magma differentiation.
- The divergence in the slab input becomes prominent at 10 Ma and can be linked to the Mariana's arc's collision with the enriched oceanic crust of the Cretaceous Western Pacific Seamount Province (WPSP) which is rich intraplate volcanoes and volcaniclastic sediments.
- The decoupling of source sensitive trends of trace elements (exemplified by $K_{4.0}$) and isotope ratios ($^{206}Pb/^{204}Pb$) suggests that collision of WPSP and Mariana arc is a multi-stage processes that may involve complex interaction of mantle flow, slab dip and plate rheology.

References

Bryant, C.J., Arculus, R.J., Eggins, S.M. (1999) Laser ablation-inductively coupled plasma-mass spectrometry and tephras: A new approach to understanding arc magma genesis. Geology, 27(12): 1119-1122.

Lee, J.M., Stern, R.J., Bloomer, S.H. (1995) Forty million years of magmatic evolution in the Mariana arc: the tephra record. J Geophys Res, 100(B9): 17671-17687.

Straub, S.M., Goldstein, S.L., Class, C., Schmidt, A. (2009) Indian-type mid-ocean ridge basalts in the northwest Pacific Ocean basin. Nature Geoscience, 2(4): 286-289, DOI: 10.1038/NGEO471.

Straub, S.M., Goldstein, S.L., Class, C., Schmidt, A., Gomez-Tuena, A. (2010) Slab and mantle controls of the Sr-Nd-Pb-Hf isotope evolution of the post-42 Ma Izu Bonin Volcanic Arc. J Petrol, 51(5): 993-1026; doi:10.1093/petrology/egq009.

Straub, S.M., Woodhead, J.D., Arculus, R.J. (2015) Temporal evolution of the Mariana Arc: mantle wedge and subducted slab controls revealed with a tephra perspective. J Petrol, 56 (2): 409-439, doi: 10.1093/petrology/egv005.

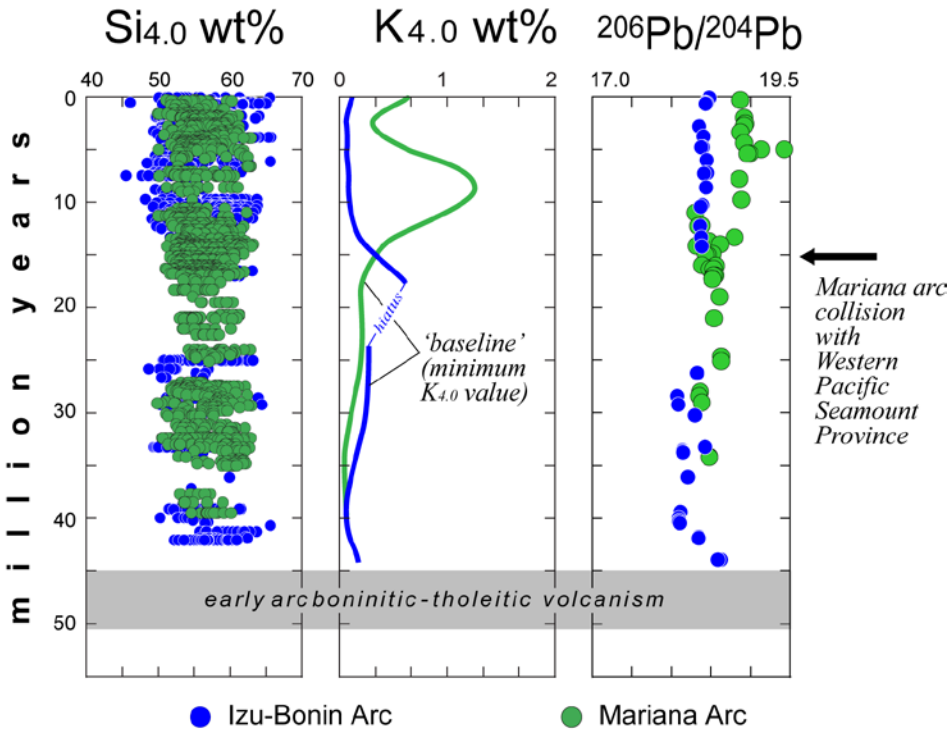

Figure 1. Tephra record of the compositional evolution of the oceanic Mariana (green) and Izu Bonin arcs (blue) in the northwest Pacific A. $Si_{4.0}$ (SiO_2 wt% normalized to 4 wt% MgO), B. minimum $K_{4.0}$ trend and C. $^{206}Pb/^{204}Pb$ isotope ratios. All tephra data from Straub et al. (2009; 2010; 2015).

Modeling Mineral Grain Size Variations in the Mantle Wedge and Its Effect on Fluid Migration

Award: 08-40800 (January 2009)

Ikuko Wada[1] and Mark D. Behn[2]

[1]Department of Earth Sciences, University of Minnesota

[2]Department of Geology and Geophysics, Wood Hole Oceanographic Institution

We developed a thermal-grain size evolution (T-GSE) model to quantify the steady-state grain size distribution in the mantle wedge. The T-GSE model couples a 2-D steady-state finite-element thermal and mantle-flow model of Wada et al. [2008] with a laboratory-derived grain size evolution model of Austin and Evans [2007], in which grain size depends on temperature and deformation conditions. We performed a suite of model calculations using idealized subduction geometries and a range of subduction parameters. All models predict significant changes in the temperature and deformation conditions over relatively short distances in the mantle wedge, giving rise to large spatial variations in grain size with a characteristic distribution, in which grain size increases down-dip from 10–100 μm at the tip of the mantle wedge corner flow to a few centimeters beneath the arc. We developed a fluid migration model that incorporates the effect of grain size variation, using the commercial finite-element package COMSOL Multiphysics. In the model, permeability depends on grain size, and fluid flow through moving mantle matrix is driven by the buoyancy of the fluids and dynamic pressure gradients induced by mantle flow. The modeling results indicate that fluids introduced along the base of the mantle wedge beneath the forearc are dragged down-dip by mantle corner flow due to small grain size and low permeability immediately above the slab. As grain size increases with depth, permeability increases, resulting in upward fluid migration beneath the expected location of the arc.

Austin N. J. and B. Evans (2007), Paleowattmeters: A scaling relation for dynamically recrystallized grain size, Geology, 35, 343-346.

Wada, I., K. Wang, J. He, and R. D. Hyndman (2008), Weakening of the subduction interface and its effects on surface heat flow, slab dehydration, and mantle wedge serpentinization, J. Geophys. Res., 113, B04402, doi:10.1029/2007JB005190.

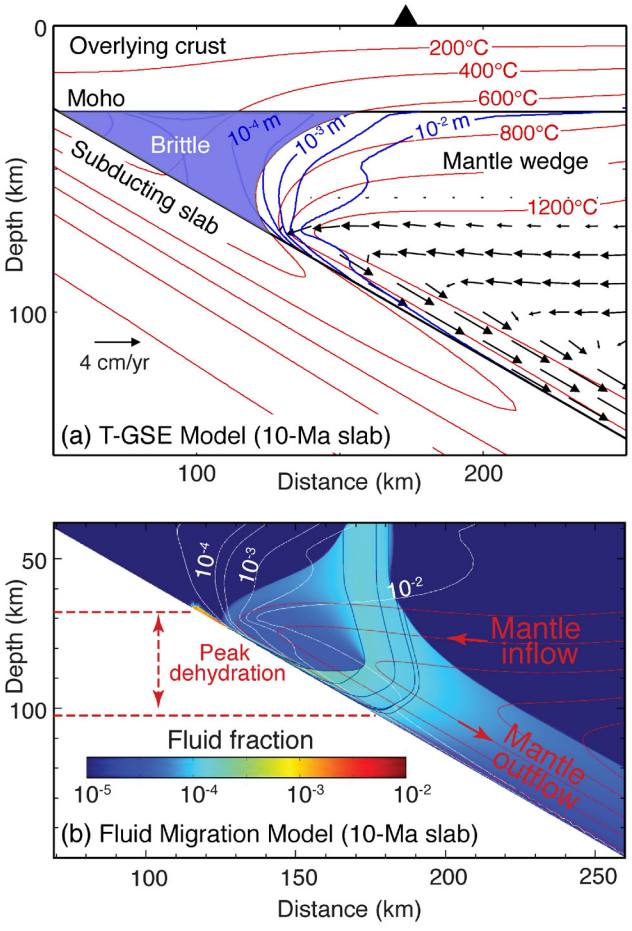

(a) Thermal filed (red contours), mantle velocities (black arrows), and grain size distribution (blue contours) calculated by a T-GSE model with a 10-Ma slab. T-GSE modeling results are not applicable to the region with temperature < 600°C (purple region) in the mantle wedge. (b) Fluid distributions (color) predicted by an FM model with a 10-Ma slab at 20 Myr after fluid influx initiation. The influx distribution is based on the patterns of H_2O release calculated for a 10-Ma slab. The grain size distribution, mantle flow field, and dynamic pressure distribution applied to the FM model are calculated by the T-GSE model shown in (a). Red horizontal dashed lines indicate the depth range of peak dehydration. Thin red and dark blue lines indicate mantle and fluid streamlines, respectively.

Project: Mantle Serpentinization and Water Cycling Through the Mariana Trench and Forearc

Douglas Wiens (Washington University) and Dan Llzarralde (WHOI)

Goals:

Major goals of this project are to test the hypothesis that substantial quantities of water are transported deep into the subduction system via upper-mantle serpentinization of the subducting plate. Complimentary goals are to delineate pathways of the water cycle in this system and quantify fluxes where possible.

Data Collection:

The initial cruise was planned for Spring 2010 but was delayed due to problems with the R/V MG Langseth. This has significantly delayed the completion of the data collection analysis. In the end 80 OBSs and 5 tethered hydrophones were deployed by the R/V Thompson in February 2012. The R/V Langseth shot its airgun array to the OBSs along 4 long lines, and also collected MCS data with a streamer (figure 1). 60 short period OBSs were then recovered by the R/V Langseth in March, 2012, leaving a passive seismic array of 20 broadband OBSs, 5 land seismographs on Northern Mariana Islands, and 5 hydrophones tethered in the water column in the deepest part of the trench. The passive array was recovered on a cruise aboard the R/V Melville in February 2013. Data return was excellent; nearly all the OBSs returned a full dataset.

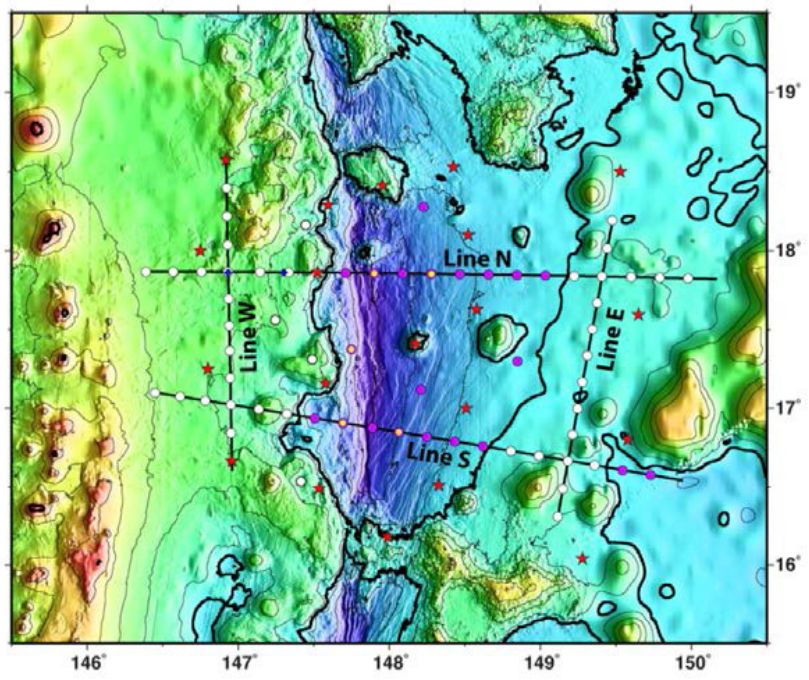

Fig. 1. Mariana Experiment layout. Symbols are: white, short-period (SP) OBS on seafloor; purple, SP OBS tethered; yellow, SP OBS tethered, year-long deployment; red star, broad-band OBS, year-long deployment. Bold contour is 5500m.

Active Source Results (Dan Lizarralde – WHOI):

Anisotropic modeling. The Mariana dataset was meant to form a major part of Nathan Miller's Ph. D. thesis. When the project was delayed, we put him to work on the anisotropic analysis of mantle refractions from beneath the outer rise offshore Nicaragua acquired during the MARGINS-funded Costa Rica cruise. That work involved substantial methodology development that benefits both projects.

A key result of the work done during the analysis of the dataset from Nicuaragua is that the anisotropic effect of large, widely spaced joints is frequency dependent. The effect is such that, offshore Nicaragua, mantle wavespeeds in the along-trench directions, parallel with plate-bending faults, are predicted to be reduced at all azimuths within the narrow frequency band of the refraction arrivals. Delay times of the mantle refraction phase, Pn, can be explained by the simple combination of inherited fabric and the effect of joints with a small contribution from thin cracks, which produce a "4-theta" azimuthal dependence. Consequently, it is possible to explain nearly all of the velocity reduction that has been observed offshore Nicaragua, in both the fast and slow direction, by the influence of jointing in the form of "altered" regions that extend out to 100m away from a given bending fault.

Reference model. Ph.D. student Helen Feng is currently finishing up work on Line E from the Mariana experiment. This line will establish the reference for the incoming plate shallow mantle velocity. This reference is particularly important since the Mariana lithosphere was modified by a large Cretaceous igneous event after its formation in the Jurassic.

The crust of the incoming plate is thicker than average oceanic crust. Even in areas with seamingly low relief, the crust is 1-2 km thicker than average. Similarly, shallow mantle velocities are slower than average oceanic mantle in both the "fast" and "slow" directions within the un-faulted region. This may represent the influence of Cretaceous volcanism. There is a distinct discontinuity at ~7 km beneath the Moho that may be related to a phase change in a basaltic component (figure 3). The strength of the contrast at that discontinuity is greater than that observed at other locations. If the discontinuity is due to a phase change from plagioclase to spinel, then the strength of the discontinuity implies a larger fraction of basaltic component impregnating the crust than is observed in other locations. This would be consistent with the uniformity of crustal thickening observed along Line E and with the somewhat slower shallow-mantle velocities observed beneath the outer rise.

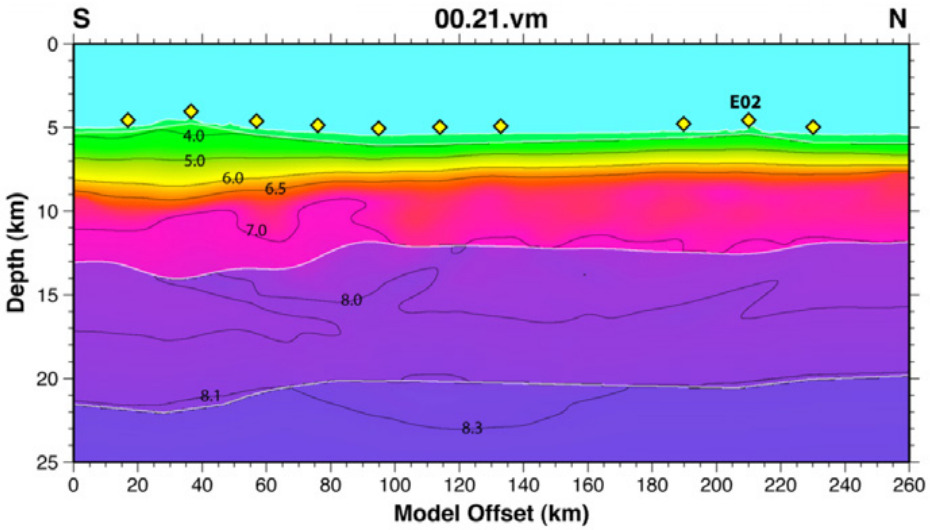

Fig. 3. Preliminary velocity model for Line E. Ph.D. student Helen Feng is currently working on this model. Line E is important because it establishes the reference crustal structure for this lithosphere, which is Jurassic age but was heavily modified by Cretaceous volcanism, and the reference upper mantle velocity in the "slow" (paleo-spreading-orthogonal) direction. A remarkable feature of this model is the distinct boundary ~7 km below the Moho (see OBS data in Fig. 4), which we interpret to be related to a plagioclase > spinel phase transition effecting a basaltic component in the mantle. The broad thickening of the crust suggests widely distributed sub-Moho Cretaceous melt.

Forearc stratigraphy. Martina Coccia, a MIT Ph.D. student, has worked up all of the MCS data from the forearc. There are many remarkable features present in the forearc dataset, with one example shown in the accompanying figure. (figure 2) Forearc stratigraphy suggests that gravity has played and continues to play an important role in evolving this margin. Active growth on extensional faults that open downslope guides serpentinite mound formation. At the same time, trench-ward moving blocks that abut stable blocks downslope have developed inverted structure, with previously extensional faults being reactivated in sequences of reverse thrusts and folds. Beneath the forearc, the seismic velocity of the mantle wedge appears to be very slow. These are complicated data and the modeling that we have done is very preliminary, but it appears that the forearc wedge is very thoroughly serpentinized. This is not terribly surprising, but we should be able to make a good measurement here, and this will be the first such measurement of this type at any arc. In addition, the forearc faults whose intersections support serpentinite-mound formation have a significant seismic velocity anomaly associated with them. This supports the notion that they are long-lived, wide deformation zones.

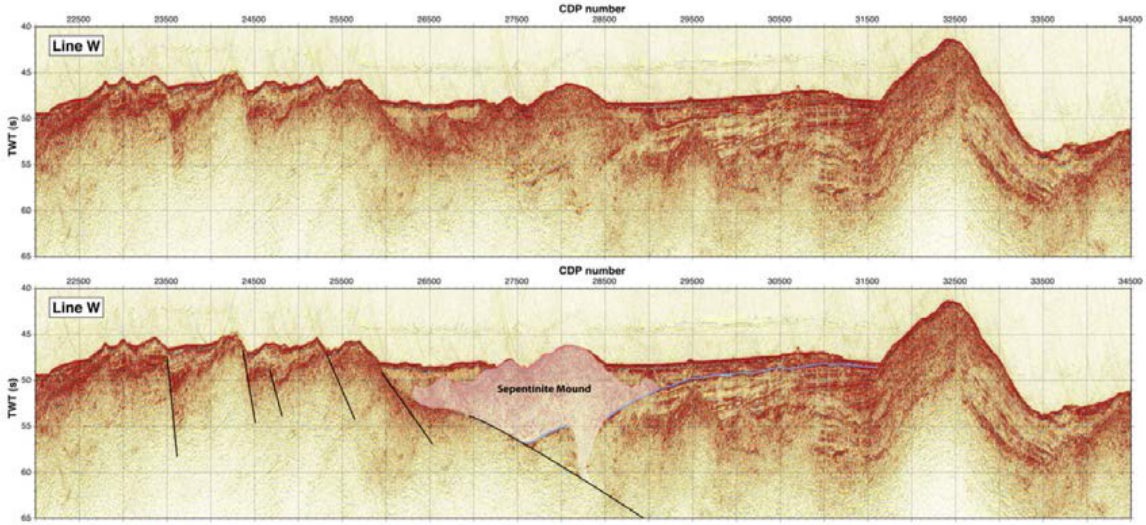

Fig. 2. Partially interpreted, migrated MCS section over a portion of Line W. These are the first images from the Mariana forearc to show subsurface structural relationships between extensional fault sets and serpentinite-mound formation. The mound indicated here is small and growing, apparently sourced by an antithetic break above a low-angle fault that has produced considerable hanging-wall rotation through time. The strike of this fault is SW-NE. The large mound to the north (cdp 32500) lies above a fault that stikes NW-SE, perpendicar to the fault beneath the small mound. These two faults intersect beneath the much larger mound east of Line W.

Passive Seismic Results (Douglas Wiens, Washington University):

Large earthquakes on the incoming plate: Because of the delay in the Mariana cruises, we began this project with graduate student Erica Emry analyzing teleseismic earthquakes on the incoming Pacific plate in the Mariana plate bending region, as well as modeling the bathymetry and stresses in this region [Emry et al., 2014]. Results from Central Mariana indicate that all earthquakes are extensional and occur at centroid depths down to 11 km below the Moho. The maximum depth of large earthquakes may extend deeper than the centroid depths and are probably limited to 15-20 km below Moho. At the Southern Mariana trench, extensional earthquakes continue to 5 km below the Moho, but one compressional earthquake at 34 km below the seafloor suggests stronger plate interface coupling here. In addition, we model the stress distribution within the Pacific plate along two bathymetric profiles extending seaward from the Mariana subduction trench axis to better understand whether our earthquake depth solutions match modeled scenarios for plate bending under applied external forces. Results from our flexure models match the locations of extensional and compressional earthquakes and suggest that the Pacific plate at Southern Mariana is experiencing larger, compressional stresses, possibly due to greater interplate coupling. Additionally, if extensional faulting promotes the infiltration of water into the subducting plate mantle, then the top 5-15 km of the Pacific plate mantle is partially serpentinized, and a higher percentage of serpeninization is located near the Central Mariana trench where extensional events extend deeper. This result formed one chapter of Erica Emry's PhD thesis (2012).

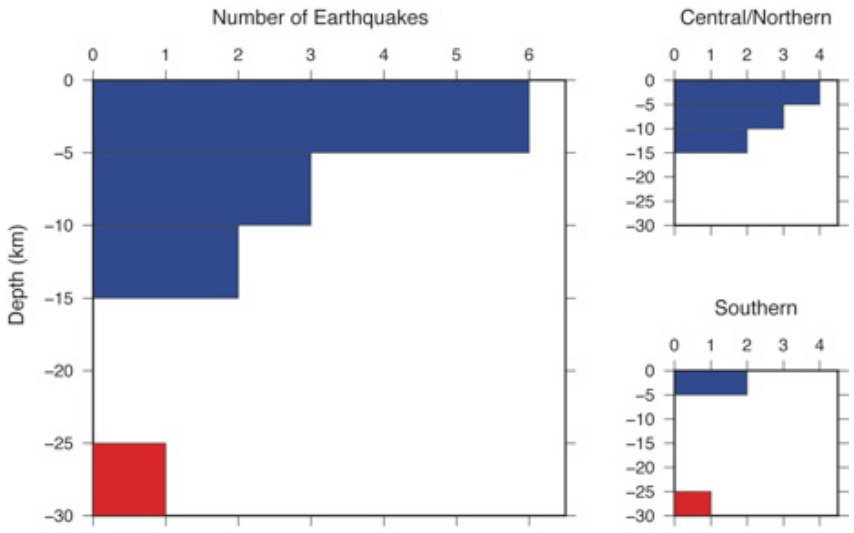

Figure 4. Distribution of earthquakes at Central/Northern Mariana with depth. Left: Depth and number of all events within the incoming Pacific plate mantle at the Mariana subduction zone. Blue bars are extensional earthquakes and red bars are compressional earthquakes. Depth is given as kilometers below the Moho. Top Right: Central Mariana earthquakes. Bottom Right: Southern Mariana. (from Emry et al., 2014)

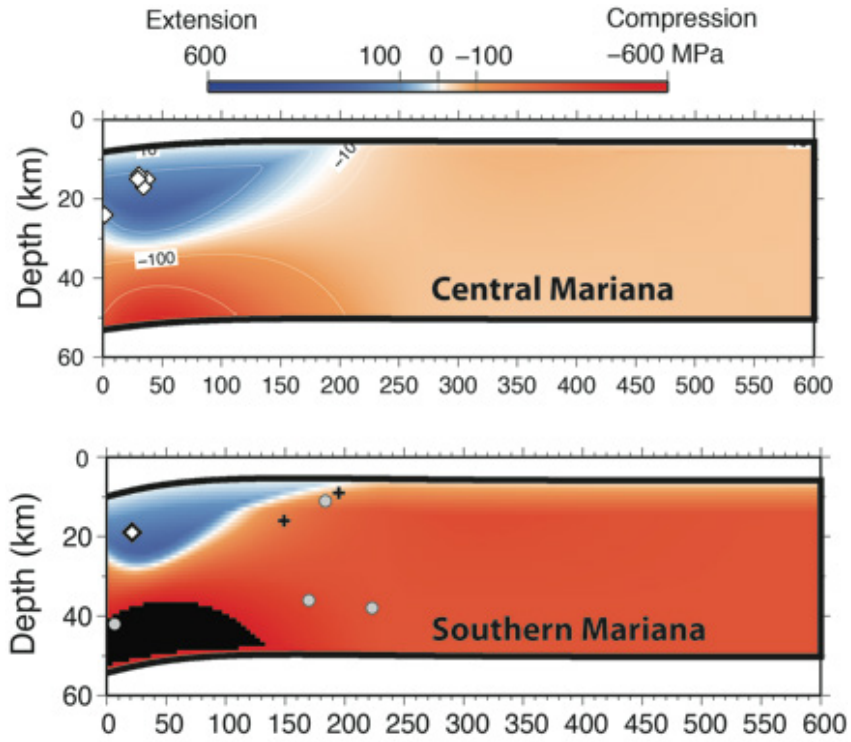

Figure 5. Top: The best-fit flexure model for the Central Mariana outer rise using bathymetry seaward (east) of the trench-axis. Bottom: The best-fit flexure model for the Southern Mariana outer rise using bathymetry seaward (southeast) of the trench-axis. Tensional deviatoric stresses correspond to blue regions and positive values (MPa); compression corresponds to red regions and negative values, and black regions indicate highly compressional stresses where the color scale has saturated. Extensional earthquakes plotted as white diamonds; strike-slip earthquakes are black crosses; compressional earthquakes are gray circles.

Microseismicity and depth of hydration on the incoming plate: Graduate student Melody Eimer and undergraduate student Hope Jasperson have been locating small earthquakes near the Mariana trench to identify the development and depth extent of normal faulting in the incoming plate, which may control the maximum depth of water circulation. Preliminary results indicate that seismicity in the incoming plate begins about 120 km east of the trench axis, with the highest seismicity levels found near the trench axis itself. The events are limited by a maximum depth of 15-25 km below the Moho, in agreement with the large earthquakes studied by Emry et al [2014]. Many of the incoming plate earthquakes locate near large fault scarps identified in seafloor bathymetry. This work formed the basis for Hope Jasperson's undergraduate honors thesis (2015).

Structure of the incoming plate from Rayleigh waves: Graduate student Chen Cai is working on determining the shear wave structure of the incoming plate from Rayleigh wave analysis, using both Rayleigh waves found in ambient noise cross-correlation as well as propagating long-period Rayleigh waves from teleseismic earthquakes. The shear velocities determined from this analysis will form an important additional constraint on physical properties when combined with the P-wave structure from active source analysis in the upper 20 km, and will extend the structural analysis to greater depths than possible with active source data. Initial results are consistent with very high velocities found in the P-wave structure at depths of 10 km below Moho within the incoming plate.

Publications:

Emry, E. L., D. A. Wiens, and D. Garcia- Castellanos, Faulting within the Pacific plate at the Mariana Trench: Implications for plate interface coupling and subduction of hydrous minerals, *J. Geophys. Res. Solid Earth, 119,* 3076–3095, doi:10.1002/2013JB010718. 2014.

Advanced models of magma migration at convergent MARGINS

Cian Wilson, Marc Spiegelman, Peter van Keken

July 17, 2015

Arc volcanism associated with subduction is generally considered to be caused by the transport in the slab of hydrated minerals to sub-arc depths. In a qualitative sense it appears clear that progressive dehydration reactions in the down-going slab release fluids to the hot overlying mantle wedge, causing flux melting and the migration of melts to the volcanic front. However, the quantitative details of fluid release, migration, melt generation and transport in the wedge remain poorly understood. In particular, there are two fundamental observations that defy quantitative modeling. The first is the location of the volcanic front with respect to intermediate depth earthquakes (e.g. 100 ± 40 km; England et al., 2004, GJI, Syracuse and Abers, 2006, G3) which is remarkably robust and insensitive to subduction parameters. This is particularly surprising given estimates on the variability of fluid release in global subduction zones (e.g. van Keken et al. 2011, JGR) which show great sensitivity of fluid release to slab thermal conditions. Reconciling these results implies some robust mechanism for focusing fluids and/or melts toward the wedge corner. The second observation is the global existence of thermally hot erupted basalts and andesites that, if derived from flux melting of the mantle requires sub-arc mantle temperatures of 1300°C over shallow pressures of 1-2 GPa which are not that different from mid-ocean ridge conditions.

These observations impose significant challenges for geodynamic models of subduction zones, and in particular for those that do not include the explicit transport of fluids and melts. Using our open source model assembler, TerraFERMA, we have developed high-resolution models that include a more complete description of coupled fluid and solid mechanics (allowing the fluid to interact with solid rheological variations) together with rheologically consistent solution for temperature and solid flow.

When driven by buoyancy alone, fluid migrates through the mantle wedge along a near vertical trajectory (see Figure 1). Only interactions with the solid flow at very low values of permeability or high values of fluid viscosity can cause deviations from this path. However, in a viscous, permeable medium, additional pressure gradients are generated by volumetric deformation due to variations in fluid flux.

Compaction pressure gradients can significantly modify the fluid flow paths (see Figure 1). At shallow depths, compaction channels form along the rheological contrast with the overriding plate while in the mantle wedge itself porosity waves concentrate the fluid. When considering multiple, distributed sources of fluid, as predicted by thermodynamic models (van Keken et al. 2011, JGR), interaction between layers in the slab itself can also cause significant focusing through high permeability channels. Acting together these three mechanisms focus fluid towards the anticipated arc location resulting in high fluxes of aqueous fluid directly beneath the arc. We estimate that this could cause $\sim 10\%$ flux melting in the sub-arc mantle wedge. This compares to the $< 1\%$ estimated to occur when only buoyancy effects are included.

In our idealized models compaction provides a mechanism for reconciling the wide distribution of fluid release when compared to the narrow, focused band of arc volcanism. However the estimated melting potential occurs at a lower temperature than petrological and geochemical constraints suggest for the final equilibration of erupted arc melts (1300°C at 1-2 GPa). Reproducing this observation in our models is an ongoing project, requiring the dynamic inclusion of melting (which was previously just estimated as a post-processing step) and possibly feedback from the fluid to the solid flow due to rheological weakening.

We are also testing the robustness of the observed focusing mechanisms across a range of subduction geometries and parameters. Further feedback between the phases may also occur through rehydration of undersaturated regions of the solid by the fluid. Initial results suggest that this may have a significant impact on the efficacy of the high permeability slab channels as a focusing mechanism.

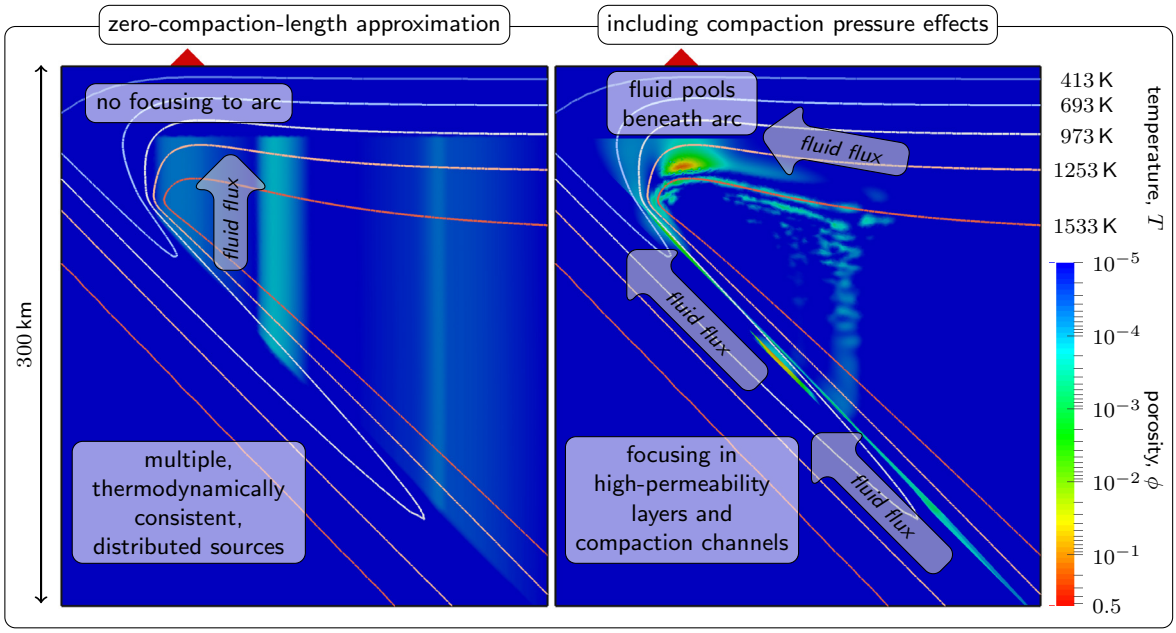

Figure 1: Fluid migration across an idealized subduction zone (Wilson et al., 2014, EPSL). In the zero-compaction-length approximation only buoyancy acts to drive fluid across the mantle wedge and hence it travels primarily vertically. With the inclusion of compaction pressure effects fluid is focused towards the idealized arc.

The range of physical behaviors described here requires a high level of flexibility in our modeling software as each setup can have different variables and equations requiring a variety of discretizations and solver strategies. To cope with this we have developed a new software infrastructure TerraFERMA (the Transparent Finite Element Rapid Model Assembler), for the rapid and reproducible description and solution of coupled multi-physics problems. TerraFERMA leverages three advanced open-source libraries for scientific computation: FEniCS, which provides high-level and highly flexible problem description, PETSc, which provides composable solvers for coupled multi-physics problems, and SPuD, which provides a science neutral options handling system. TerraFERMA integrates these libraries into an easier to use interface that organizes all scientific and computational choices into a single options file, from which a custom compiled application is generated and run. Because all models share the same infrastructure, they become more reusable and reproducible. TerraFERMA is open source and available as a developers release at http://terraferma.github.io. It has been benchmarked against numerous geodynamic benchmarks relevant to these problems (see Figure 2).

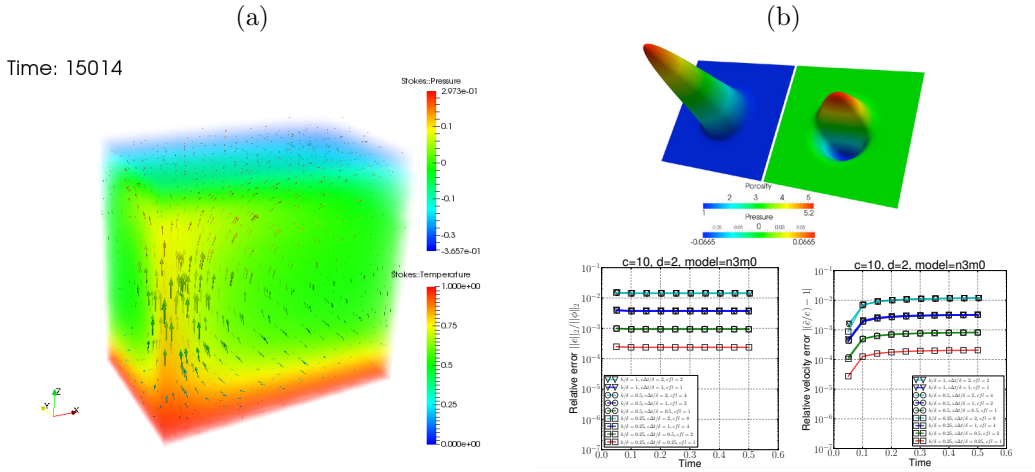

Figure 2: Example benchmark results produced using TerraFERMA. (a) Three-dimensional thermal convection from Busse et al., 1994, Geophys. Astro. Fluid. (b) Magma solitary waves from Simpson & Spiegelman, 2011, J. Sci. Comput.

References acknowledging GeoPRISMS

- Kramer, S. C., Wilson, C. R., Davies, D. R. (2012). An implicit free surface algorithm for geodynamical simulations. Physics of Earth and Planetary Interiors.

- Le Voci, G., Davies, D. R., Goes, S., Kramer, S. C., Wilson, C. R. (2013) A systematic 2-D investigation into the mantle wedge's transient flow regime and thermal structure: complexities arising from a hydrated rheology and thermal buoyancy. Geochemistry, Geophysics, Geosystems.

- Wilson, C. R., Spiegelman, M., Van Keken, P. E. (2014). Fluid flow in subduction zones: the role of solid rheology and compaction pressure. Earth and Planetary Science Letters.

- Garel, F., Goes, S., Davies, D. R., Davies, J. H., Kramer, S. C., Wilson C. R. (2014) Interaction of subducted slabs with the mantle transition-zone: A regime diagram from 2-D thermo-mechanical models with a mobile trench and an overriding plate. Geochemistry, Geophysics, Geosystems.

- Tosi, N., Stein, C., Noack, L., Hüttig, C., Maierová, H., Davies, D. R., Wilson, C. R., Kramer, S. C., Thieulot, C., Glerum, A., Fraters, M., Spakman, W., Rozel, A., Tackley, P. J. (2015) A community benchmark for viscoplastic thermal convection in a 2-D square box. Geochemistry, Geophysics, Geosystems.

- Jones, T.D., Davies, D. R., Campbell, I. H., Wilson, C. R., Kramer, S. C. (submitted) From Plume Source to Hotspot: Do Mantle Plumes Preserve the Heterogeneous Structure of their Deep-Mantle Source? Earth and Planetary Science Letters.

Tectonic Reconstruction of the Gulf of California–Salton Trough (GCAST) Plate Boundary

Scott E.K. Bennett [1,2]; Lisa A. Skinner [3]; Michael H. Darin [3,4]; Paul J. Umhoefer [3]; Michael E. Oskin [1]; Rebecca J. Dorsey [4]

[1] University of California–Davis; [2] U.S. Geological Survey; [3] Northern Arizona University; [4] University of Oregon

Results from a decade of NSF-MARGINS science in the Gulf of California–Salton Trough (GCAST) rift, the focus site of the Rupturing Continental Lithosphere initiative, necessitated a synthesis of the current state of knowledge. To fulfill this need, we constructed a series of digital, GIS-based, paleotectonic and paleogeographic maps and animations that track development of the GCAST plate boundary in 1-million-year increments from 11 Ma to the present (Bennett et al., 2013).

The GCAST region is an excellent example of successful continental rupture leading to sea-floor spreading and formation of conjugate rift margins. Continental rupture in the GCAST region occurred along the core of the Gulf of California Shear Zone (Bennett and Oskin, 2014), a belt of localized, high-strain dextral transtension that became embedded within a broader region of diffuse, low-strain extension, as Pacific-North America (PAC-NAM) relative motion became more oblique ca. 8 Ma. This narrow belt hosted increased crustal thinning and subsidence, leading to the punctuated, fault-controlled, south-to-north flooding of the Gulf seaway ca. 8 to 6 Ma (Umhoefer et al., 2013). Still, contrasting models left several unanswered questions about the timing of rift initiation, timing of marine incursion, total offset across the Gulf, and kinematics of plate boundary development.

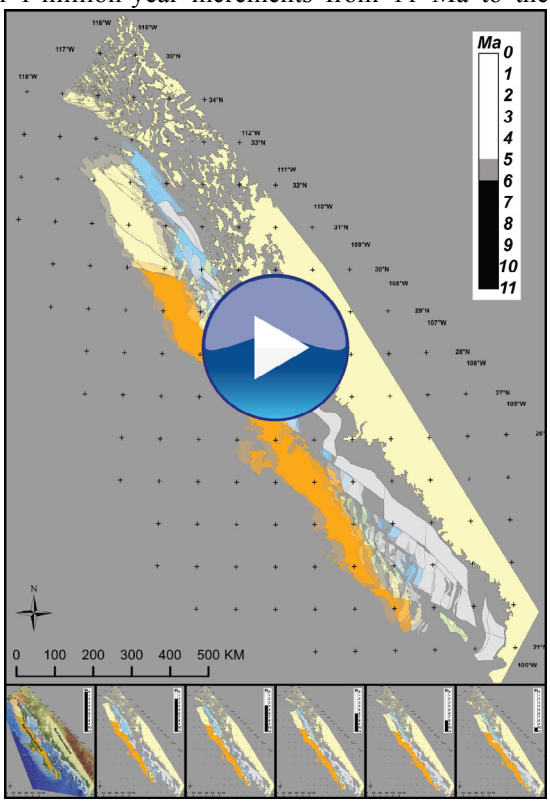

Figure: Animations of GCAST tectonic reconstruction (upper panel) are assembled from 1 Myr 'time-slices' of detailed palinspastic tectonic maps (lower panels). Video: https://youtu.be/aQn9ZsrbPUg

To fully explore the implications and evaluate the validity of existing plate boundary models, we devised three GCAST reconstructions (Bennett et al., 2013), varying the percent-coupling between the Baja California microplate and the North America plate. Our reconstructions honor the results from scores of studies that either pre-date or were funded by the MARGINS program. A fundamental constraint is the recently revised global plate circuit, which requires ~550 km of total PAC-NAM relative plate motion since 11 Ma, accommodated on structures across the GCAST region, including west of Baja California and in coastal mainland Mexico. Geodetic studies indicate that contemporary PAC-NAM relative motion remains partitioned, with ~10% still accommodated west of Baja California. Extensive, pre-rift geologic deposits serve as piercing points across the Gulf and results from marine geophysical studies (gravity and seismic lines) constrain the extent of submerged continental crust. Transects across the PAC-NAM plate boundary offer reconciliation of cumulative offset across the southern San Andreas fault (Darin and Dorsey, 2013) and estimate the distribution of post-Miocene deformation across the PAC-NAM plate boundary (Darin et al., 2013). Numerous field-based geologic studies document the finer-scale timing and kinematics of rift-related fault zones and sedimentary basins (Keogh, 2010; Darin, 2011; Bennett, 2013), the distribution of dextral shear related to oblique rifting (Bennett and Oskin, 2014), and the timing of marine incursion (Bennett et al., 2015).

Looking forward, these GCAST reconstructions highlight remaining gaps in our current understanding of the distribution, timing, style, and magnitude of PAC-NAM plate boundary deformation and identify locations where future research is needed to address unresolved controversies. Synthesis and reconstruction of the early Gulf seaway provides critical input for other scientific fields, such as geogenomic and phylogenic studies that evaluate the role of rifting and seaway formation on divergent evolution and biologic diversity across the Gulf (Dolby et al., in press). GCAST reconstructions play an integral role in the development of college curriculum, including open-source mini-lessons related to the GCAST region (Lamb et al., 2014; Loveless et al., 2014) cultivated during the early years of the GeoPRISMS program.

Papers, Theses, and Abstracts Resulting From This NSF-MARGINS Study
(* indicates peer-reviewed publication)

Bennett, Scott E.K., Skinner, Lisa A., Darin, Michael H., Umhoefer, Paul J., Oskin, Michael E., and Dorsey, Rebecca J., 2013, New Constraints on Baja California-North America Relative Plate Motion Since 11 Ma, American Geophysical Union, Fall Meeting 2013, abstract #T14C-02.

Bennett, S.E.K., 2013, The role of rift obliquity in formation of the Gulf of California [Ph.D. thesis]: Davis, California, University of California–Davis, 220 p.

* Bennett, S.E.K., and Oskin, M.E., 2014, Oblique rifting ruptures continents: Example from the Gulf of California shear zone: Geology, v. 42, p. 215–218, doi: 10 .1130 /G34904.1

* Bennett, S.E.K., Oskin, M.E., Dorsey, R.J., Iriondo, A., and Kunk, M.J., 2015, Stratigraphy and structural development of the southwest Isla Tiburón marine basin: Implications for latest Miocene tectonic opening and flooding of the northern Gulf of California: Geosphere, v. 11, no. 4, doi: 10 .1130 /GES01153.1.

Darin, M.H., 2011, Late Miocene extensional deformation in the Sierra Bacha, coastal Sonora, México: Implications for the kinematic evolution of the Proto–Gulf of California [M.S. thesis]: Eugene, Oregon, University of Oregon, 95 p.

* Darin, M.H., and Dorsey, R.J., 2013, Reconciling disparate estimates of total offset on the southern San Andreas fault. Geology, v. 41 no. 9 p. 975-978.

Darin, Michael H., Bennett, Scott E.K., Oskin, Michael E., and Dorsey, Rebecca J., 2013, Cumulative Dextral Strain Across The Miocene-Present Pacific-North America Plate Boundary: Eastern California Shear Zone To The Northern Gulf Of California, Geological Society of America Abstracts with Programs. Vol. 45, No. 6, p.22

* Dolby, G.A., Bennett, S.E.K., Lira-Noriega, A., Wilder, B.T., and Munguia-Vega, A., in press, Assessing the geological and climatic forcing of biodiversity and evolution surrounding the Gulf of California, Journal of the Southwest.

Keogh, M., 2010, Stratigraphic analysis of Late Miocene to Early Pliocene(?) sedimentary rocks, SW Isla Tiburón, Sonora, Mexico [B.S. Honors Thesis]: Eugene, Oregon, University of Oregon, 76 p.

Lamb, Melissa A., Cashman, Susan M., Bennett, Scott E.K., Loveless, John P., Goodliffe, Andrew M., and Dorsey, Rebecca J., 2014, A New Curriculum Using Cutting Edge Scientific Results from the MARGINS-GeoPRISMS Program, Rupturing Continental Lithosphere Part I: introducing seismic interpretation and isostasy principles using Gulf of California examples, American Geophysical Union, Fall Meeting 2014, abstract #ED51D-3453.

Loveless, John P., Bennett, Scott E.K., Cashman, Susan M., Dorsey, Rebecca J., Goodliffe, Andrew M., and Lamb, Melissa A., 2014, Incorporating Cutting Edge Scientific Results from the MARGINS-GeoPRISMS Program into the Undergraduate Curriculum, Rupturing Continental Lithosphere Part II: introducing Euler poles using Baja-North America relative plate motion across the Gulf of California, American Geophysical Union, Fall Meeting 2014, abstract #ED51D-3455.

Umhoefer, Paul J., Skinner, Lisa A., Bennett, Scott E.K., Oskin, Michael E., Dorsey, Rebecca J., and Darin, Michael H., 2013, Breaching of Transform faults and flooding of pull-apart basins to incrementally form the early Gulf of California seaway from ~8 to 6.3 Ma, Geological Society of America Abstracts with Programs. Vol. 45, No. 6, p.15.

Geodetic Quantification of Active Tectonics of the S Red Sea-Afar Depression

Robert Reilinger

As part of our broader study of the southern Red Sea/Afar Depression, supported in part by GeoPRISMS, we used geodetic, plate tectonic, and geologic observations to quantitatively reconstruct the geologic evolution of the Red Sea and Gulf of Aden since separation of Arabia from Africa in the Late Oligocene (Reilinger et al., 2015). Rifting initiated at 22 ± 3 Ma roughly simultaneously along the full strike of the proto-Red Sea and Gulf of Aden. Rifting began along pre-existing zones of weakness associated with a Pan-African Precambrian collisional suture shortly after the Afro-Arabia Plate was weakened by impingement of the African hot spot (~30 Ma). The initial phase of continental rifting followed a roughly linear trend from the Gulf of Suez in the north, to the Bab-al-Mandab in the south where the Afar Triple Junction (junction of Red Sea, Gulf of Aden, and East African rifts) was located at that time. The initial rate of extension across the rift was roughly half the present-day rate. At 11 ± 2 Ma, the rate of rifting doubled to the present-day rate (24 ± 1 mm/year in the south [~12°N] and 7 ± 1 mm/year in the north [~27°N]) and the configuration of rifting changed in both the northern and southern Red Sea. This time corresponds to the initiation of ocean spreading (i.e., complete severing of the continental lithosphere and intrusion of rift basalts) along the full extent of the Gulf of Aden. The changes in the S Red Sea involved the propagation of the Afar Triple Junction westward to its present location (~11.5°N, 42°E), the transfer of rifting from the S Red Sea (Bab-al-Mandab) to the more N–S oriented Danakil Depression, and accompanying CCW rotation of the Danakil Block with respect to Africa. In the northern Red Sea, rifting transferred from the Gulf of Suez to the more N–S-oriented Gulf of Aqaba/Dead Sea fault system. The rate of rifting has not changed significantly since that time (i.e., 11 ± 2 Ma). The initiation of rifting at 22 ± 3 Ma corresponds temporally with slowing of Africa–Eurasia convergence by a factor of ~2 and the changes at 11 ± 2 Ma with a second phase of slowing of Africa–Eurasia convergence, while Arabia–Eurasia convergence has remained roughly unchanged since >30 Ma. These observations are consistent with simple models where changes in Africa–Arabia–Eurasia relative plate motions are the fundamental cause of post-Oligocene Middle East and Mediterranean tectonics. Based on the simultaneity between full ocean spreading along the Gulf of Aden and a doubling of the extension rate across the Red Sea, and the change to more N–S-oriented rifting in both the northern and southern Red Sea, we hypothesize that slowing of Africa–Eurasia convergence resulted from a decrease in slab pull on the African Plate across the evolving AR-AF plate boundary.

Reilinger, R.E., S. McClusky, and A. ArRajehi, Geodetic constraints on the geodynamic evolution of the Red Sea (in) The Red Sea: Formation, Morphology, Oceanography, and Environment of a Young Ocean Basin, (editors) N. Rasul and I.C.F. Stewart, Springer Publishing, 135-149, 2015.

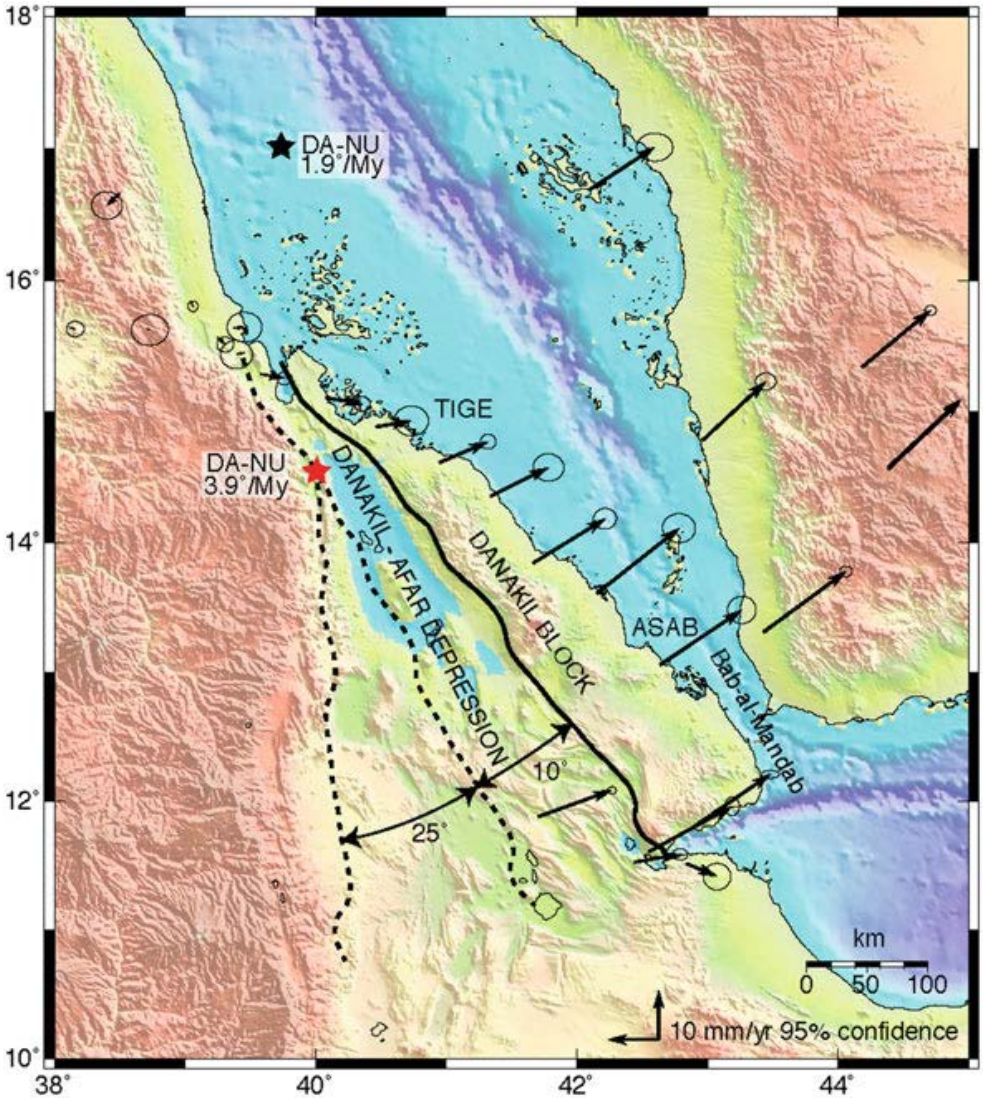

Back-rotation of the western side of the Danakil Block (represented by the solid black line) around the GPS Danakil–Nubia (DA–NU) rotation pole (black star at ~17°N) to initial overlap of unextended terrains (at ~15°N) after 10° rotation (~5 Ma; easternmost dashed line). A second back-rotation around a proposed pole near the location of initial overlap (red star) of an additional 25° (westernmost dashed line) closes the Danakil Depression. Full closure is achieved at 11 ± 2 Ma.

GeoPRISMS Science Nugget “Controls on Magma Generation at Incipient Spreading Centers”

Axel K. Schmitt (University of California, Los Angeles)

Geochronologic and geochemical studies of igneous rocks are essential to constrain the mechanics of magmatic rifting via establishing process rates and detecting the nature of the magmatic sources at depth. For incipient spreading centers such as the Gulf of California – Salton Trough region, constraints on ages and compositions of magmas are difficult to come by because of the youthful nature of the rocks, and the widespread alteration in environments of intense geothermal activity and rapid sedimentation. The goal of this study was to reliably establish ages and sources for surface and subsurface (from geothermal wells) magmatic rocks from the Salton Trough and northern Gulf of California. We focused on the use of zircon as an alteration resistant phase that permits direct dating and insights into the chemical compositions of its host magmas. The major results that superseded and complemented existing data for this region are (Schmitt et al., 2013a; 2013b):

- Volcanism in the Salton Trough is much younger than previously assumed; new (U-Th)/He zircon ages for the Red Hill rhyolite dome at the southeastern end of the modern Salton Sea indicate a late Holocene (ca. 2.5 ka) eruption which implicates the region as volcanically active;
- Late Pleistocene magmatism at the surface and in the subsurface was dated for Cerro Prieto and Wagner basins adjacent to the south of the Salton Trough;
- Rift-related magmatism is fundamentally oceanic in character as is evident by overlapping neodymium isotopic compositions between the most mafic rocks from the Salton Trough-northern Gulf of California and those from active spreading centers of the East Pacific Rise;
- Evolved (dacitic to rhyolitic) magmatism is largely unrelated to melting of pre-existing continental crust, or sediments;
- Remelting of hydrothermally altered basalt, similar to oceanic environments such as Iceland, is the dominant mechanism that produces evolved magmas;
- Deep-reaching hydrothermal convection of surface waters is an important process to be considered in thermal models of magmatic rifting.

Subsequent studies led by the USGS California Volcano Observatory (Wright et al., 2015) have confirmed that volcanism in the Salton Sea is mid to late Holocene in age, and that rhyolite domes erupted in three separate episodes.

Project-related References:

Schmitt, A. K., Martín, A., Stockli, D. F., Farley, K. A., & Lovera, O. M. (2013a). (U-Th)/He zircon and archaeological ages for a late prehistoric eruption in the Salton Trough (California, USA). Geology, 41(1), 7-10.

Schmitt, A. K., Martín, A., Weber, B., Stockli, D. F., Zou, H., & Shen, C. C. (2013b). Oceanic magmatism in sedimentary basins of the northern Gulf of California rift. Geological Society of America Bulletin, 125(11-12), 1833-1850.

Citations discussing research funded by GeoPRISMS

Carley, T. L., Miller, C. F., Wooden, J. L., Padilla, A. J., Schmitt, A. K., Economos, R. C., ... & Jordan, B. T. (2014). Iceland is not a magmatic analog for the Hadean: Evidence from the zircon record. Earth and Planetary Science Letters, 405, 85-97.

Cooper, K. M. (2015). Timescales of crustal magma reservoir processes: insights from U-series crystal ages. Geological Society, London, Special Publications, 422, SP422-7.

Hauksson, E., Stock, J., Bilham, R., Boese, M., Chen, X., Fielding, E. J., ... & Yang, W. (2013). Report on the August 2012 Brawley Earthquake Swarm in Imperial Valley, Southern California. Seismological Research Letters, 84(2), 177-189.

Wright, H. M., Vazquez, J. A., Champion, D. E., Calvert, A. T., Mangan, M. T., Stelten, M., ... & Schriener, A. (2015). Episodic Holocene eruption of the Salton Buttes rhyolites, California, from paleomagnetic, U-Th, and Ar/Ar dating. Geochemistry, Geophysics, Geosystems, 16(4), 1198-1210.

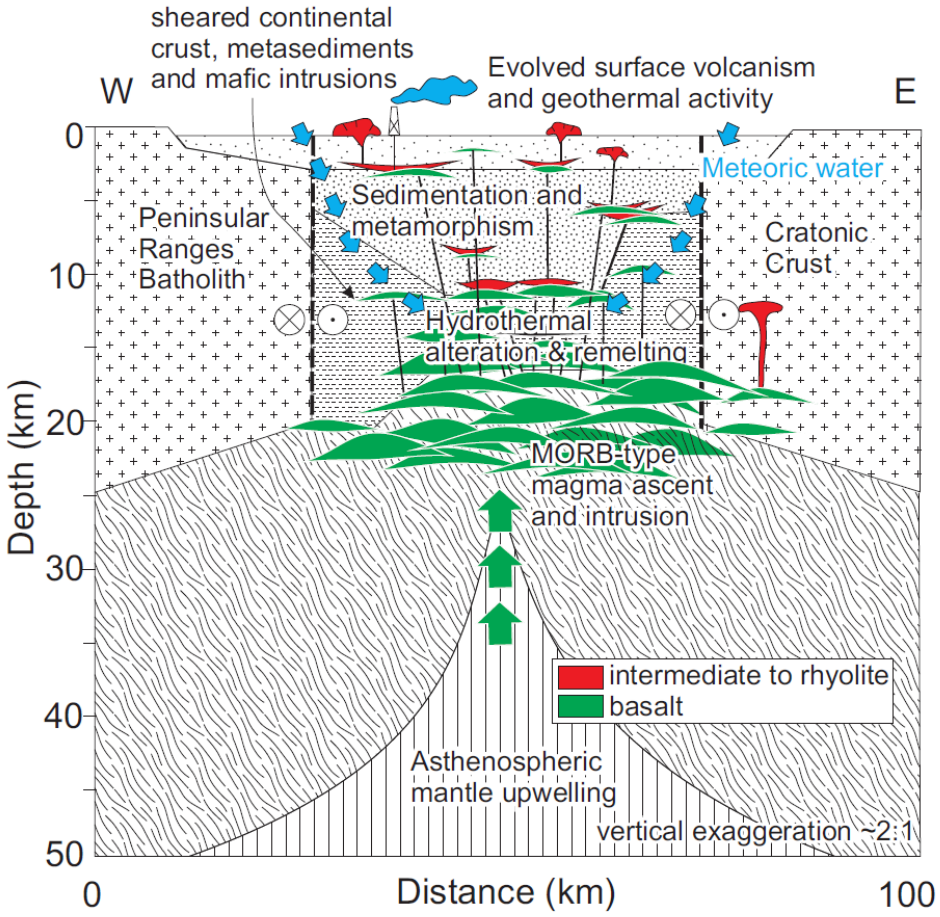

Figure 1. Schematic cross section illustrating the magmatic processes in northern Gulf of California rift basins. Active magmatism involves mid-ocean-ridge basalt (MORB)-type parental magmas derived from partial melting of decompressing asthenosphere, with intermediate and rhyolitic magmas generated by fractional crystallization and remelting of hydrothermally altered mafic intrusions. Circulation of meteoric waters is schematically indicated. The depth of melting is constrained by geothermal drilling to be > 3 km.

Long-term morphodynamic evolution of the Lower Fly River (Papua New Guinea)

Alberto Canestrelli, Sergio Fagherazzi

Department of Earth and Environment, Boston University, Boston, MA 02143, USA

We used a one-dimensional morphodynamic model to analyze the long-term evolution of the lower reaches of the Fly River, Papua New Guinea, from the Everill Junction to the delta mouth. The model shows how the break in the exponential trend of river width triggers deposition, thus producing a tidal region characterized by a higher bed elevation with respect to the river-dominated one. Numerical simulations indicate that the river attains a dynamic equilibrium configuration in which the amount of sediment entering upstream is flushed seaward. The model shows that the equilibrium configuration results from a delicate balance between the aggrading effect associated with channel divergence (acting mainly during neap tide and at slack water) and the opposite effect of tidal flushing driven by residual water discharge. A physically meaningful morphodynamic equilibrium occurs only for a small range of values of sediment discharge prescribed at the upstream boundary. In particular, an increase in sediment discharge leads to aggradation, while a decrease triggers extensive scour and a deepening of the estuary.

Published Manuscripts

Canestrelli A., S. Lanzoni, and S. Fagherazzi (2014), One-dimensional numerical modeling of the long-term morphodynamic evolution of a tidally-dominated estuary: The Lower Fly River (Papua New Guinea), Sedimentary Geology, 301, 107-119, 10.1016/j.sedgeo.2013.06.009.

Canestrelli A., Fagherazzi S., Lanzoni S. (2012) A mass-conservative centered finite volume model for solving two-dimensional two-layer shallow water equations for fluid mud propagation over varying topography and dry areas, Advances in Water Resources, Volume 40, Pages 54-70

Canestrelli, A., & Toro, E. F. (2012). Restoration of the contact surface in FORCE-type centred schemes II: Non-conservative one-and two-layer two-dimensional shallow water equations. Advances in Water Resources, 47, 76-87.

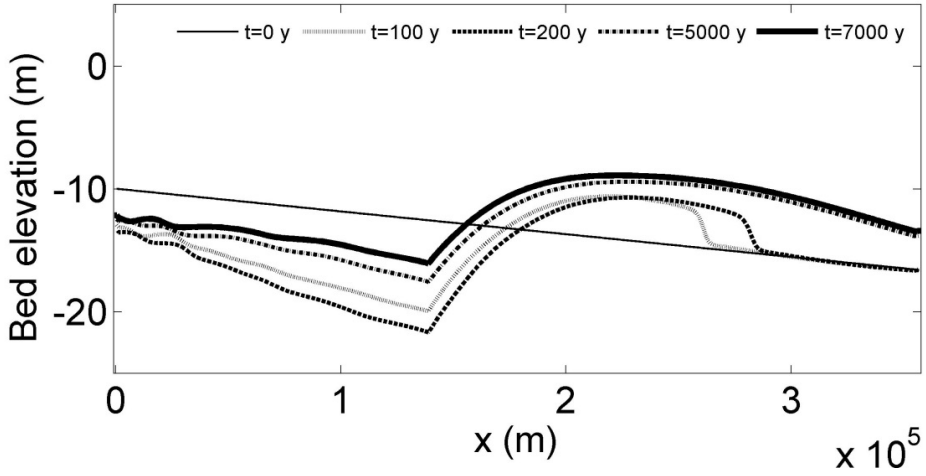

Figure 1. Bed level of the lower Fly River at five different instants of the long-term evolution. The point at km 0 represents the Everill Junction while the delta starts around km 150. The initial bottom profile is linear.

A Source to Sink Perspective of the Waipaoa River Margin

Steven A. Kuehl[a], Clark R. Alexander[b], Neal E. Blair[c,k], Courtney K. Harris[a], Kathleen M. Marsaglia[d], Andrea S. Ogston[e], Alan R. Orpin[f], Joshua J. Roering[g], Aaron J. Bever[h], Eric L. Bilderback[i], Lionel Carter[j], Corina Cerovski-Darriau[g], Laurel B. Childress[k], D. Reide Corbett[l], Richard P. Hale[m], Elana L. Leithold[n], Nicola Litchfield[o], Julia M. Moriarty[a], Mike J. Page[o], Lila E. R. Pierce[a], Phaedra Upton[o], John P. Walsh[l]

[a] *Virginia Institute of Marine Science, College of William and Mary, Gloucester Point, VA 23062, USA*
[b] *Skidaway Institute of Oceanography, University of Georgia, Savannah, GA 31411, USA*
[c] *Department of Civil and Environmental Engineering, Northwestern University, Evanston, IL 60208, USA*
[d] *Geological Sciences, California State University Northridge, Northridge, CA 91330, USA*
[e] *School of Oceanography, University of Washington, Seattle, WA 98195, USA*
[f] *National Institute of Water and Atmospheric Research (NIWA), Private Bag 14-901, Kilbirnie, Wellington, New Zealand*
[g] *Department of Geological Sciences, University of Oregon, Eugene, OR 97403, USA*
[h] *Anchor QEA, LLC, San Francisco, CA 94102*
[i] *Geologic Resources Division, National Park Service, Denver, CO 80225, USA*
[j] *Antarctic Research Centre, Victoria University of Wellington, PO Box 600, Wellington, New Zealand*
[k] *Department of Earth and Planetary Sciences, Northwestern University, Evanston, IL 60208, USA*
[l] *East Carolina University, UNC Coastal Studies Institute, Greenville, NC 27858, USA*
[m] *Department of Earth and Environmental Sciences, Vanderbilt University, Nashville, TN 37235, USA*
[n] *Department of Marine, Earth, and Atmospheric Sciences, North Carolina State University, Raleigh, NC 27695, USA*
[o] *GNS Science, PO Box 30-368, Lower Hutt 5040, New Zealand*

Keywords: Waipaoa River, New Zealand, continental margin, sedimentology, stratigraphy, landscape evolution, sediment transport, carbon cycle

ABSTRACT

A fundamental goal of the Earth Science community is to understand how perturbations on Earth's surface are preserved in the stratigraphic record. Recent Source to Sink (S2S) studies of the Waipaoa Sedimentary System (WSS) are synthesized herein to provide a holistic perspective of the processes that generate, transport and preserve sedimentary strata and organic carbon on the Waipaoa margin in the late Quaternary. Rapid uplift associated with subduction processes and weak sedimentary units have conspired to generate rapid rates of incision and erosion in the Waipaoa catchment since the Last Glacial Maximum (LGM). We show that although much of the sediment exported offshore during this time interval originated from valley excavation, a substantial portion emanated from hillslopes, mostly through deep-seated landslide and earthflow processes that were vigorous during periods of rapid fluvial incision just prior to the Pleistocene-Holocene transition. Lacustrine sediments deposited in naturally-dammed 7-ky-old Lake Tutira provide a record of Holocene environmental controls on upper catchment sedimentation in the WSS. 1400 storms are identified, with one storm period (1830–2030 cal.

BP) of particularly high magnitude and frequency. Storm frequency is modulated by the waxing and waning of atmospheric teleconnections between the tropics and Antarctica. Furthermore, clear long-term changes in sediment yield are evident from the Lake Tutira record following human settlement as conversion to pasture is accompanied by a 3-fold increase in the long-term lake sediment accumulation rate.

Whereas there is ample evidence that Waipaoa River flood deposits are routinely deposited offshore in the sheltered confines of Poverty Bay, over the longer term, waves and currents subsequently resuspend and transport these deposits both landward (coarse fraction) and seaward (fine fraction). Thus, the timing of sediment supply to areas of net sediment accumulation is more often driven by wave events that are not associated with river flooding. Therefore, we conclude that asynchronicity of river-sediment delivery and of wave resuspension in most instances precludes the direct preservation of flood events in the stratigraphic record of the Waipaoa Shelf. Over the longer term, the sediment package preserved on the shelf and slope since the LGM can be explained in large measure by sequence-stratigraphic models forced by varying sea level and ongoing tectonic deformation of the margin. As sea level rose, sediment supply to the slope was reduced by about a factor of 5 due to shelf trapping. Despite this reduction, turbidites are found at similar frequency throughout the LGM-Present, as the dominant trigger appears to be subduction earthquakes, with large ones having a return interval of about 200 $\pm$ 100 years. Sediment-budget exercises that consider both modern (river discharge versus centennial accumulation rates) and post-LGM (terrestrial production versus offshore isopachs) mass balances indicate that about half of the total sediment production from the Waipaoa escapes the study area. Moreover, a coupled sediment transport-hydrodynamic shelf model and observations of textural trends on the shelf indicate that a large fraction of the sediment is carried outside the study area along the shelf to the northeast by the river plume or by combined current/wave activity. Therefore, we conclude that the WSS is an open system with sediment escape from the present day through the LGM.

The organic matter associated with sediment as it moves from upland source to marine sink is a product of particle history, and provides a record of materials that have cycled over timescales of days to millions of years. The ubiquity of fossil Organic Carbon (OC) in both the terrestrial and marine realms of the Waipaoa attests both to the chronic nature of its source, crumbling mudstones further destabilized by landuse, and its biogeochemical recalcitrance. Modern OC persists by virtue of its continual production along the S2S transit. The Waipaoa, like other small mountainous rivers on active margins, exhibits a high riverine OC preservation efficiency (>50%) in its marine depocenter because of the rapid, event-driven accumulation of sediment. The Waipaoa contrasts with dispersal systems on wide, energetic shelves (e.g., the Amazon and Fly Rivers) where sediment is extensively refluxed in oxygenated overlying water resulting, in the biogeochemical incineration of particulate OC.

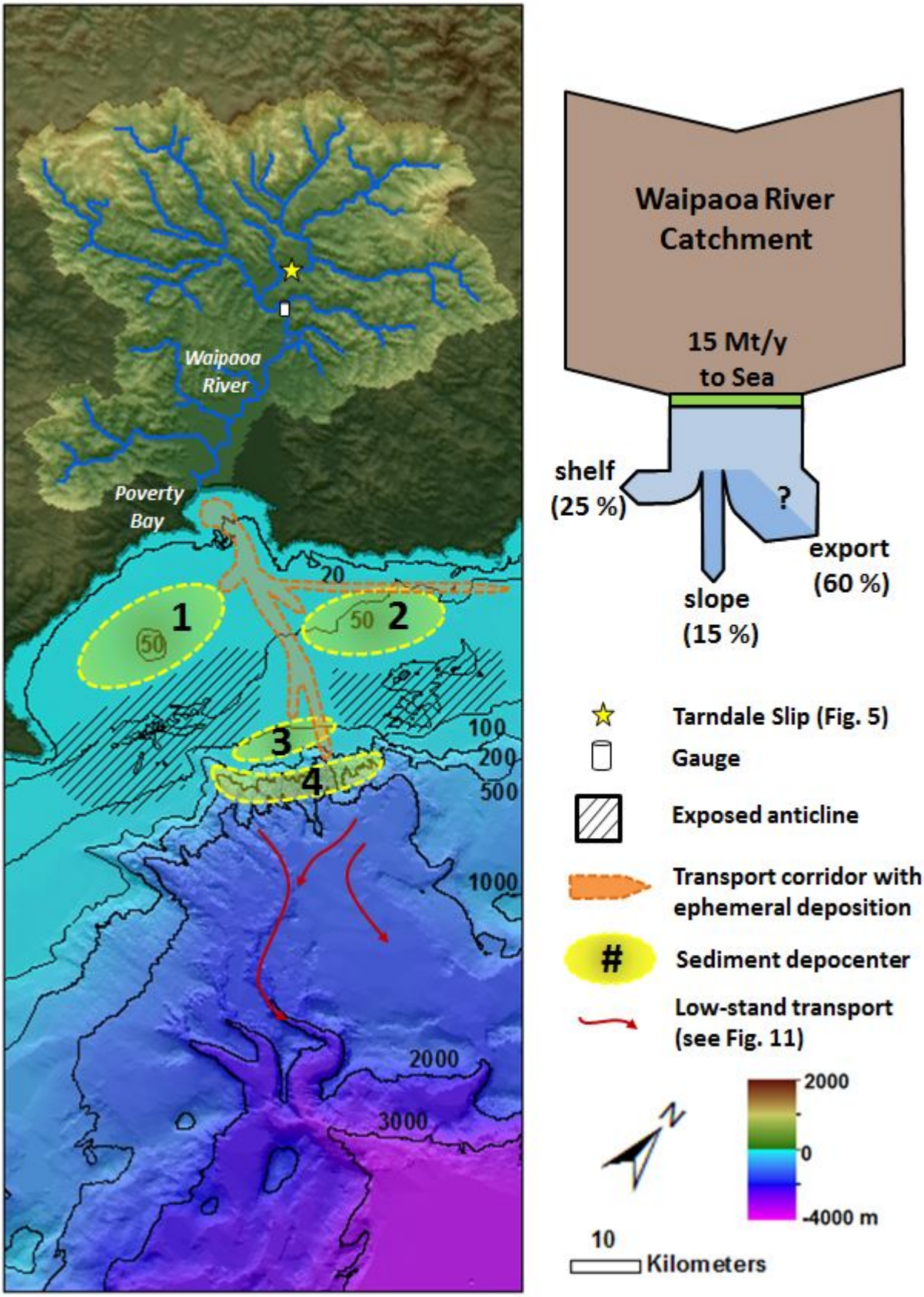
Waipaoa River
Catchment
15 Mt/y
to Sea
shelf
(25 %)
?
export
(60 %)
slope
(15 %)
Waipaoa
River
Poverty
Bay
1
2
3
4
20
50
50
100
200
500
1000
2000
3000
Tarndale Slip (Fig. 5)
Gauge
Exposed anticline
Transport corridor with
ephemeral deposition
Sediment depocenter
Low-stand transport
(see Fig. 11)
2000
0
-4000 m
10
Kilometers

Rapid Landscape Evolution and Sediment Production in the Waipaoa River Basin since the Last Glacial Maximum

J. Roering (PI), C. Cerovski-Darriau (PhD Student), E. Bilderback (co-PI)

The active tectonic setting and weak geologic substrate of the Waipaoa Sedimentary System (WSS) promoted profound and extensive morphologic change and sediment export since the last glacial maximum (LGM). A robust and comprehensive sediment budget for the terrestrial component of the WSS is required for comparison with the timing and magnitude of downstream sediment dispersal and deposition in the offshore environment (Kuehl et al., in press). Modern sediment fluxes are dominated by gully processes, but landforms in the Waipaoa demonstrate that a range of post-LGM erosional processes were pervasive, including valley excavation and diverse mass wasting processes. Post-LGM incision of the mainstem Waipaoa channel incited widespread downcutting throughout the tributary network, which in turn triggered a diffuse pattern of landsliding, a significant component of terrestrial sediment production. The combination of remote sensing data, particularly airborne lidar topography and air photo mapping, with field-based data, including tephrochronology, has provided us with a powerful means to quantify trends in sediment production that can be synthesized with the sediment dispersal and depositional components of this well-studied source-to-sink system.

In the Waipaoa, post-LGM landscape change was neither steady nor uniform. Rather, scattered portions of the landscape (mostly in the headwaters) contain relict 'Pleistocene' hillslopes as knickpoints downstream demarcate the up-catchment extent of post-LGM fluvial network adjustment. Incision commenced within 1 ky following the termination of the LGM, averaging 1-3 mm y^{-1} except for a period of rapid incision (7-10 mm y^{-1}) around the Pleistocene-Holocene (~11.5 ka) transition. During this 2-4 ky interval of rapid lowering, a disproportionate fraction (40-60%) of post-LGM incision was accomplished. Post-LGM fluvial incision and vegetation change, as well as post-European settlement deforestation, promoted extensive hillslope adjustment via landsliding that continues today. Currently, a spectrum of landslide styles can be found in the Waipaoa and these account for much of the sediment delivered to the Waipaoa since the post-LGM climate shift and in response to recent land-use change (Bilderback et al., 2014).

Deep-seated landslide activity varies from slow, relatively continuous deformation to catastrophic failure. In many situations, tephra deposits combined with landslide maps indicate that ridgelines have migrated or lowered up to 100 m since the LGM due to slide activity (Bilderback et al., 2014). Deep failures tend to emerge (or daylight) along the hillslope-valley interface where basal slip surfaces are sometimes visible, suggesting that local base-level lowering facilitates gravitational collapse for the vast majority of features (Bilderback et al., 2014). In particularly weak geologic units in the Waipaoa (e.g., relict fault zones or mélange), slow-moving earthflow complexes reduce slope gradients and imprint flow-like features across the landscape surface (Fig. 5D). These mass movements resemble elongate (>100 m) sediment 'glaciers' and seldom exceed 10 m in depth. Despite modest slope angles (<10 degrees), earthflows translate downslope at rates of 10^0 to 10^1 m y^{-1}.

On terraces or landslide surfaces, the age assigned to the basal tephra observed in soil pits or hand-auger samples corresponds to the timing of the first eruption since that location was last disturbed by landsliding, or duration since stabilization (Bilderback et al., 2014). Using tephrochronology to establish the minimum age of surfaces disrupted by landsliding, Bilderback (2012) determined that >20% of Waipaoa hillslopes have been affected by landsliding since the LGM and demonstrated that widespread hillslope adjustment occurred 9-13 ka, coincident with the period of rapid incision. Taken together, post-LGM terrestrial sediment sources equate to an average denudation rate of 0.8 mm y^{-1}, consistent with the range of rock uplift values observed in the Waipaoa basin. However, this volume of sediment produced greatly exceeds the mass tallied from the Waipaoa floodplain and marine sediments

of the adjacent shelf and slope, implying that post-LGM transport out of the continental shelf may be substantial.

Data that quantify temporal variations in hillslope erosion since the LGM are limited. Comparison of a post-LGM landscape erosion analysis for a Waipaoa tributary (Mangataikapua) (Cerovski-Darriau et al., 2014) with fluvial incision rates and the initiation of widespread deep-seated landsliding (Bilderback et al., 2014) confirm that peak terrestrial-sediment production occurred around the Pleistocene-Holocene transition. These observations suggest that slope failure and hillslope-derived sediment production are tightly coupled with incision and valley excavation. Furthermore, the post-LGM erosion rate of >1.6 mm y^{-1} for the 16-km^2 earthflow-dominated Mangataikapua tributary catchment is associated with a narrow band of weak early Cretaceous melange, indicating that variations in rock type can modulate landslide erosion rate by a factor of 2 or more (Bilderback et al., 2014; Cerovski-Darriau et al., 2014).

References:

Cerovski-Darriau, C., Roering, J., Marden, M., Palmer, A., Bilderback, E., 2014. Quantifying temporal variations in landslide-driven sediment production by reconstructing paleolandscapes using tephrochronology and lidar: Waipaoa River, New Zealand. G-cubed: Geochem. Geophys., Geosy., doi: 10.1002/2014GC005467.

Bilderback, E. L., 2012. Hillslope response to climate-modulated river incision and the role of deep-seated landslides in post-glacial sediment flux: Waipaoa Sedimentary System, New Zealand, PhD. Thesis, University of Canterbury, http://hdl.handle.net/10092/7439.

Bilderback, E. L., Pettinga, J., Litchfield, N. J., Quigley, M., Marden, M. , Roering, J. J., Palmer, A. S., 2014. Hillslope response to climate-modulated river incision in the Waipaoa Catchment, East Coast North Island, New Zealand, Geol. Soc. of Am., doi:10.1130/B31015.1.

Kuehl, S.A., C.R. Alexander, N.E. Blair, C.K. Harris, K.M. Marsaglia, A.S. Ogston, A.R. Orpin, J.J. Roering, A. Bever, E. L. Bilderback, L. Carter, C. Cerovski-Darriau, L.B. Childress, D.R. Corbett, R. Hale, E.L. Leithold, N. Litchfield, J. Moriarty, M.J. Page, L. E.R. Pierce, P. Upton, and J.P. Walsh, (in press), A Source to Sink Perspective of the Waipaoa River Margin, Earth Science Reviews.

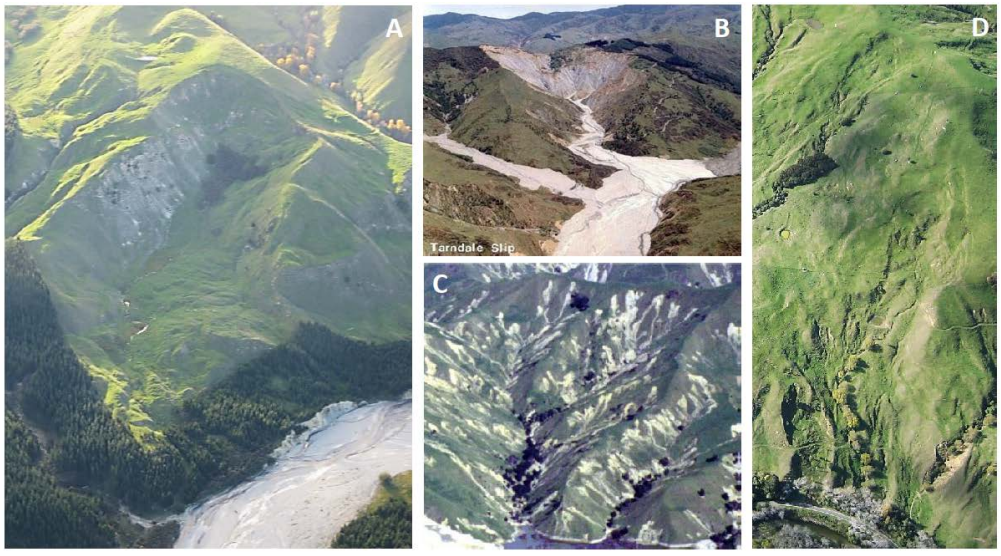

Figure 1 - Photos of common sediment production processes in the Waipaoa River watershed. A) Deep-seated landslides often displace pre-LGM surfaces and deliver sediment to channels, photo by A. Booth, B) Many gullies, like the well-known Tarndale Slip, became common after European settlement and expanded in area leading to downstream aggradation and high sediment yields, photo by Ministry for Primary Industries, New Zealand, C) Shallow landslides like these triggered by the 1988 Cyclone Bola mobilize the soil mantle, photo by M. Page, and D) Slow-moving earthflows impart a fluid-like appearance to hillslopes and generate rapid slope relaxation in response to incision, photo by J. Roering.

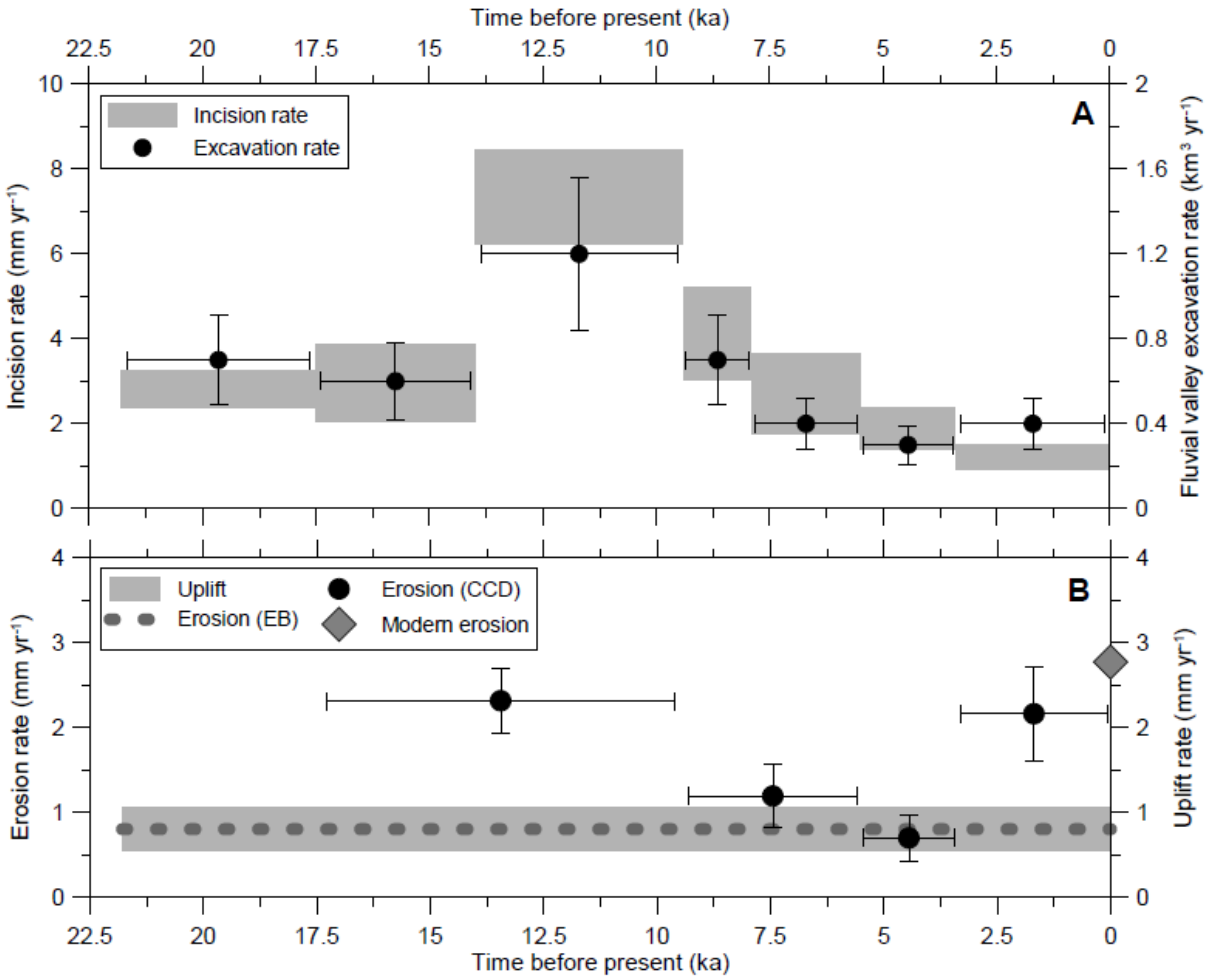

Figure 2 - Post-LGM temporal variation in rates of landscape change. A) Average fluvial incision rate (gray boxes) and volumetric valley excavation rate (filled black circles) peak around the Pleistocene-Holocene transition (9-13ka) before declining through the Holocene. Shaded box width and horizontal error bars represent the temporal sampling interval defined by tephra deposits used to establish terrace ages. Shaded box height and vertical error bars represent one standard deviation of the incision rate. Modified from Marden et al., 2014. B) Average post-LGM erosion rate for two catchments in the upper Waipaoa (labeled EB, dashed dark gray line, Bilderback, 2012) overlap with the average uplift rate estimated by Berryman et al. (2000) and Litchfield and Berryman (2006). Variation of erosion rate (labeled CCD, filled black circles) for the earthflow-dominated, Mangataikapua catchment (Cerovsk-Darriau et al., 2014). Note that high erosion rates coincide with rapid incision before declining through the Holocene and approaching the uplift rate. In the late Holocene, erosion increases, partly due to the anthropogenic role in slope destabilization. Modern erosion rates (filled gray diamond) estimated by suspended-sediment data (Hicks et al., 2000) exceed uplift and average erosion rates by nearly a factor of 4.

Sediment Gravity Flows and Variability in Sedimentation:
Key Insights from the Waipaoa River Continental Shelf (New Zealand)

PIs: J.P. Walsh[1], D. Reide Corbett[1], Courtney K. Harris[2], Andrea S. Ogston[3], Alan R. Orpin[4]

The accumulating areas of continental margins record past events, and can be analyzed to infer a region's geologic or recent history (Corbett et al., 2014). However, to interpret continental shelf strata we must understand marine sedimentary processes that impact the seabed over modern timescales. The marine dynamic processes that move sediment from riverine sources to their ultimate sink are spatially and temporally complex because oceanic, climatic, and tectonic processes vary across continental margins. The oceanographically energetic and geologically active Waipaoa River margin of New Zealand provided a great opportunity to investigate the link between active transport processes and associated depositional signatures in the stratigraphic record.

Observations and numerical models have garnered insights into how sediment transport impacts dispersal and deposition on the Waipaoa continental shelf. The river empties into a tectonically created embayment where transport processes have a major influence on initial sediment dispersal (Fig. 1A). The bay acts as a temporary deposition zone for river-derived material, with reworking and export of sediment occurring during subsequent wave events (Bever et al., 2011). Thus, delivery of sediment to the coastal ocean is generally asynchronous with its final deposition in the Waipaoa system, except in the case of long-duration (> 120 hr) storms when large ocean waves accompany high river discharge (Hale et al., 2014; Hale and Ogston, in review). This disconnect between flood delivery and storm emplacement leads to a high degree of variability in deposition for short, event time-scales (Kniskern et al., 2014; Walsh et al., 2014).

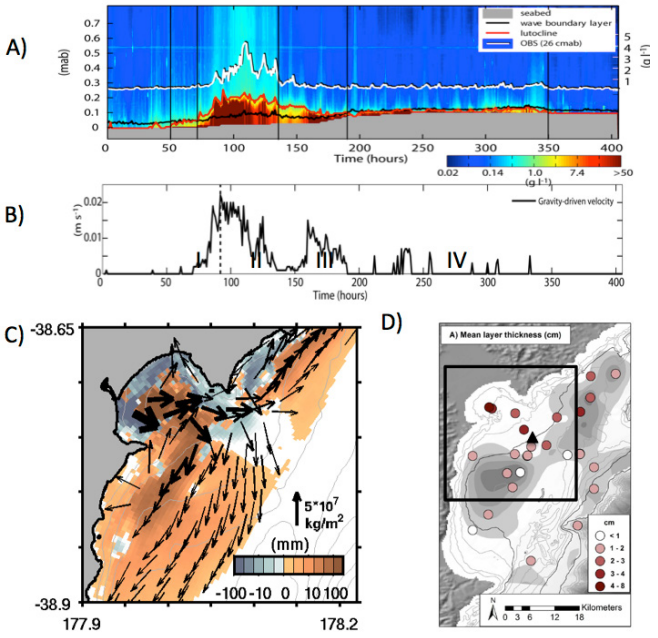

Figure 1. A) Nearbed suspended-sediment concentration during a wave-supported gravity flow that coincided with the July, 2010 flood. B) Estimated across-shelf speed of the wave-supported gravity flow. C) Modeled seabed erosion and deposition (color) and sediment flux (vectors) for July, 2010. D) Circles represent estimated event-layer thickness using ^{7}Be for the same time period from Walsh et al. (2014). Triangle in (D) approximates location of tripod observations in (A – B), and the box identifies area shown in (C).

Comparison of modeled and observed short-term deposition on the shelf with the time-averaged pattern of shelf accumulation highlights how stochastic event-dispersal behavior can often differ from the longer-term sedimentary strata (Moriarty et al., in review; Walsh et al., 2014). On the continental shelf, material accumulates in slightly deeper shelf areas where wave bed shear stress and resuspension is reduced. Areas of low average bed stresses are co-located with mid-shelf depocenters over century-to-Holocene timescales (Miller and Kuehl, 2010; Gerber et al., 2010). In this manner, the bed-stress patterns inferred

from modern waves and currents can be related to longer-term depositional patterns (Moriarty et al. in review).

Additionally, observations and models shed light on the role of wave-supported gravity flows (e.g., fluid muds; Fig. 1C, D). When flood and storm events coincide, wave-supported fluid muds can move sediment from the inner shelf to the mid shelf, and, if conditions persist, can transport sediment off of the continental shelf. The deposits associated with these flows were clearly identified in x-radiographs of the seabed, but the resulting seabed signature appeared to vary spatially (Fig. 2). Both observations and model results suggested that on the Waipaoa shelf, sediment gravity flows are a critical part of the transport and important for routing sediment from the inner shelf to deeper areas, including longer-term depocenters (Hale and Ogsten, in review).

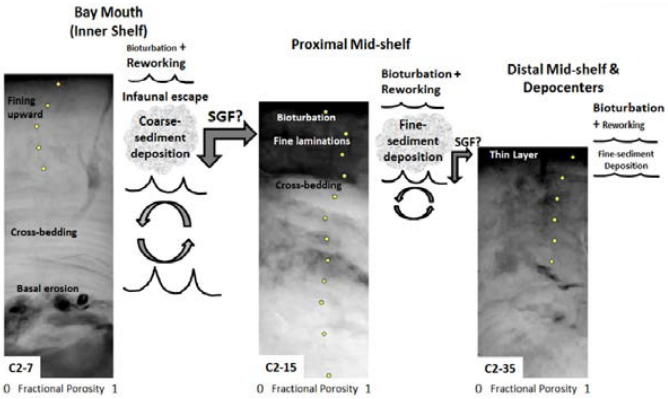

Figure 2. Example of cross-shelf stratigraphy potentially resulting from a sediment gravity flow (SGF; Walsh et al., 2014).

PUBLICATIONS (*graduate student first author)

*Bever, A.J., McNinch, J.E. and Harris, C.K., 2011. Hydrodynamics and sediment-transport in the nearshore of Poverty Bay, New Zealand: Observations of nearshore sediment segregation and oceanic storms. Cont. Shelf Res., 31(6), 507-526.

Bever, A.J., Harris, C.K., 2014. Storm and fair-weather driven sediment-transport within Poverty Bay, New Zealand, evaluated using coupled numerical models. Cont. Shelf Res, 86:34-51.

Bever, A.J., Harris, C.K., In preparation. Sensitivity of sediment dispersal and sorting to basin geometries: A case study of Poverty Bay, New Zealand.

Corbett, D.R., Walsh, J.P., Harris, C.K., Ogston, A.S., Orpin, A.R. (2014) Formation and preservation of sedimentary strata from coastal events: Insights from measurements and modeling. *Cont. Shelf Res* 86:1-5.

*Hale, R.P., Ogston, A.S., Walsh, J.P., Orpin, A. (2014) Sediment transport and event deposition on the Waipaoa River shelf, New Zealand. *Cont. Shelf Res* 86:52-65.

*Hale, R., Ogston, A.S. (in review) In-situ observations of wave-supported fluid-mud generation and deposition on an active continental margin. *JGR Earth Surface.*

Kniskern, T.A., Mitra, S., Orpin, A.R., Harris, C.K., Walsh, J.P., Corbett, D.R., 2014. Characterization of a flood-associated deposit on the Waipaoa River shelf using radioisotopes and terrigenous organic matter abundance and composition, Cont. Shelf Res, http://dx.doi.org/10.1016/j.csr.2014.04.012.

Kuehl, S.A., Alexander, C.R., Blair, N.E., Harris, C.K., Marsaglia, K.M., Ogston, A.S., Orpin, A.R., Roering, J.J., Bever, A., Bilderback, E.L., Carter, L., Cerovski-Darriaug, C., Childress, L.B., Corbett, D.R., Hale, R.P., Leithold, E.L., Litchfield, N., Moriarty, J.M., Page, M.J., Pierce, L.E.R., Upton, P., Walsh, J.P. (in review) A Source to Sink Perspective of the Waipaoa River Margin. *Earth Sciences Reviews*.

*Moriarty, J.M., Harris, C.K., Hadfield, M.G., 2014. A hydrodynamic and sediment transport model for the Waipaoa Shelf, New Zealand: Sensitivity of fluxes to spatially-varying erodibility and model nesting. J. Mar. Sci. Eng., 2: 336-369.

*Moriarty, J.M., Harris, C.K., Hadfield, M.G., In Review. Event-to-seasonal sediment dispersal on the Waipaoa River shelf, New Zealand: a numerical modeling study. Submitted to Cont. Shelf Res, August, 2014.

*Moriarty, J.M., Harris, C.K., Friedrichs, C.T., In Preparation. Gravity-driven transport on the Waipaoa River Continental Shelf, New Zealand.

Walsh, J.P., Corbett, D.R., Kiker, J., Orpin, A., Hale, R., Ogston, A. (2014) Spatial and temporal variability in sediment deposition and seabed character on the Waipaoa River margin, New Zealand. *Cont. Shelf Res* 86:85-102.

Collaborative Research: Defining locations and patch sizes for slow earthquake ruptures in subduction zones

PIs Bilek, DeShon, Engdahl

Subduction zone earthquakes exhibit a wide range of rupture behaviors that can impact the amount of damage they cause. Great M 9 subduction megathrust earthquakes, such as the 2004 Sumatra and 1964 Alaska, generate devastating large tsunami with their large co-seismic fault displacements. Other smaller magnitude (between M_w 7 and 8) earthquakes, otherwise known as tsunami earthquakes, generate large tsunami that are unexpected given the reported size of the event. These events, such as the 1992 Nicaragua tsunami earthquake, typically have slow or long duration ruptures that may be a function of displacements within patches of low strength materials along the fault zone. Some smaller magnitude earthquakes share similar long duration rupture characteristics with the tsunami events. These smaller earthquakes are interesting because they occur in most of the world's subduction zones, not just in the few regions of past tsunami earthquakes. If these two classes of earthquakes share a common mechanism of rupture through weaker material, then mapping out zones of slow earthquake occurrence would provide valuable information on possible tsunami hazards.

Our project characterized spatial variations in the rupture processes within subduction zones (Figure 1) by determining rupture parameters for events using refined locations in global subduction zones and addressing the following questions:
1) Are slow earthquakes common in known tsunami earthquake zones?
2) Are there other areas within global subduction zones that produce these slow ruptures? If so, what are the characteristics of these areas (size of rupture areas, frequency of slow rupture, etc)?
3) Are there any correlations between regions with seismically slow earthquakes and aseismic processes, such as ETS or afterslip, in subduction zones?

We find long duration events in regions of past tsunami earthquakes in over decadal time scales (Figures 2 and 3 as examples). This spatial correlation is not observed in tsunami earthquake zones along Alaska, Kuriles, and Peru. These decadal patterns in certain regions are intriguing, suggesting that the causes of these long duration/tsunami earthquakes are present over long time periods. The lack of consistency with all regions of past tsunami earthquakes suggests a need to look at differences between the margins.

Another key finding is the lack of correlation between rupture duration and sediment type or thickness. We find long duration events in subduction zone segments that range from little (< 200 m) to thick (> 1.5 km) pelagic or terrigenous sediments in the trench. This is an important result, as previous research has suggested connections between the tsunami earthquakes and sediment subduction. Our work suggests that sediment thickness and type cannot be the primary influence on the rupture velocity and duration of earthquakes. There is a stronger correlation between location of long duration events and presence of subducting features, such as fracture zones and seamounts. This aspect is worthy of further study to better understand if fluid flow within these features can impact the earthquakes along these regions. There is also a weak correlation between long duration events and areas of afterslip, particularly in regions of Sumatra and Kuriles. This suggests similar conditions are required for both afterslip and long duration events.

Our results support overall downdip variations in duration as observed previously, although in many areas, we find some long duration events at deeper extents of the seismogenic zone. These deeper long duration events are interesting, especially in light of recent observations of depth dependent seismic radiation in great subduction zone earthquakes such as 2011 Japan. Our examples of long duration (lower frequency radiation) events at the downdip end should help to constrain possible explanations for the cause of dominantly high frequency seismic radiation seen in the larger events at the deeper portions of the megathrust.

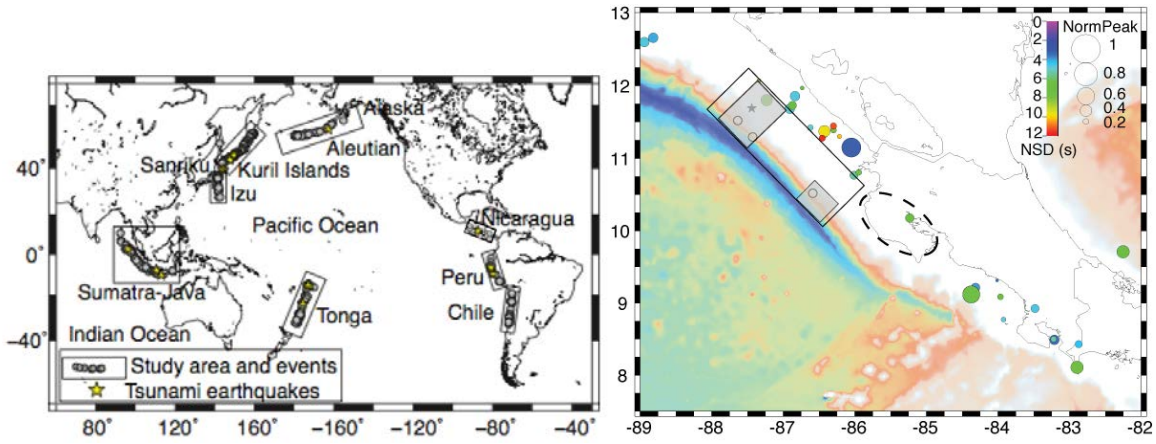

Figure 1 (left). Map of study regions and events analyzed in study. Figure 2 (right). Nicaragua/Costa Rica source parameter results. Long duration events (circles colored by normalized source duration (NSD), red being the longest duration) are concentrated in the region of the 1992 Nicaragua tsunami earthquake (rupture area outlined by black box outline, gray shaded boxes are areas of high slip during 1992). Dashed outline is area of slow slip and tremor along Nicoya Peninsula, with 1 longer than margin average earthquake in that zone.

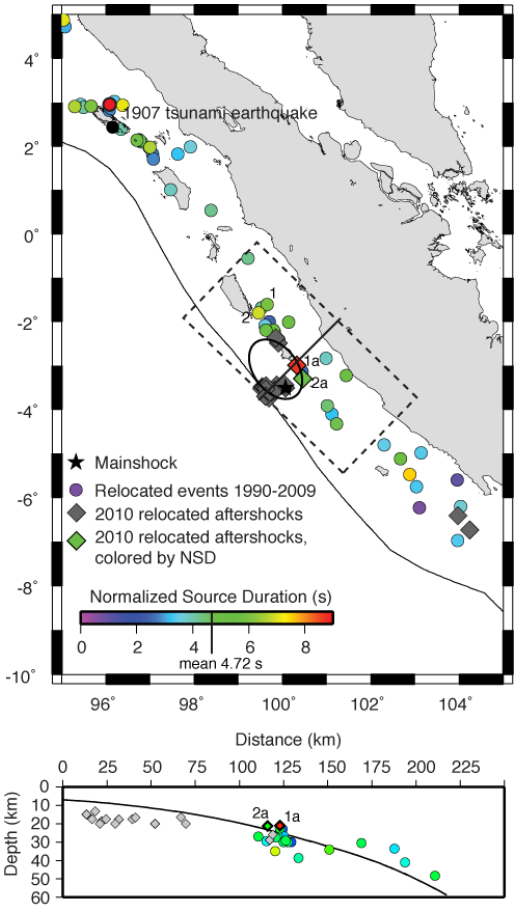

Figure 3. Source parameters for the 2010 mainshock (star shows relocated epicenter; solid ellipse shows rupture extent estimated from body and surface wave analysis), relocated earthquakes from 1990-2009 (circles, colored by NSD), and relocated aftershocks (diamonds, grey, or colored by NSD where available). Events 1 and 2 are long duration events in 2005 (1) and 2007 (2). Events 1a and 2a are the long duration aftershocks. Aftershocks defined by time relative to mainshock. NSD of the mainshock is ~18 s, higher than shown in the color bar. Dashed box outlines area of cross section. b) Cross section across the 2010 epicentral region showing relocated aftershocks (grey diamonds) primarily in the updip portion of the seismogenic zone. A small number of aftershocks also occurred within the 20-30 km depth region, two of which (1a and 1b, diamonds colored by NSD) had long normalized rupture durations, similar to the mainshock and older events (circles colored by NSD) at the northern extent of the rupture zone. Slab position (solid line) based on Slab 1.0 model [Hayes and Wald, 2009]. Figure from Bilek et al. [2011].

Collaborative Research: A Plate Boundary Observatory on the Nicoya Peninsula, Costa Rica

Tim Dixon, Susan Schwartz

The great megathrust earthquakes and tsunamis of 2004 (Sumatra) and 2011 (Japan) were reminders that our ability to forecast earthquake magnitude and tsunami risk remains weak. Subduction zone megathrust earthquakes, which tend to be the largest and generate the most destructive tsunamis, are especially problematic because the critical zone of strain accumulation often lies far offshore and is difficult to characterize with on-land sensors. It is also unclear what controls rupture area, which influences earthquake magnitude, and rupture depth, which influences tsunami potential.

Seismic and geodetic observations on the Nicoya Peninsula of northwest Costa Rica, originally funded by NSF's Margins program, and now by core programs in EAR and OCE, are aimed at addressing these issues. The peninsula overlies a shallow portion of the megathrust fault, providing sensitivity to seismic loading and release in the critical up-dip (shallow) part of the seismogenic zone. Seismicity and surface displacements associated with the September 5, 2012 M_w 7.6 Nicoya earthquake [*Yue et al.,* 2013; *Protti et al*., 2014 as well as pre-earthquake slow slip events [*Outerbridge et al.,* 2010; *Jiang et al.*, 2012] and after-slip [*Malservisi et al*., 2015] were well-recorded. The rupture area of the earthquake can be related to the area of pre-earthquake strain accumulation [*Feng et al.,* 2012].

Slow slip events (SSEs) and associated seismic tremor are proving to be an important part of subduction zone earthquake studies [*Schwartz and Rokosky*, 2007; *Beroza and Ide*, 2011]. In Nicoya, pre-earthquake slow slip appears to bear some relation to the subsequent earthquake rupture area [*Dixon et al.,* 2014; Figure 1]. Areas that experienced significant slow slip prior to the earthquake did not experience seismic rupture in the 2012 event. If this behavior is characteristic of other subduction zones, it suggests that better monitoring of SSEs could provide useful information for earthquake and tsunami forecasting. If on the other hand it occurs only in specific regions, it may give clues to the various frictional processes that ultimately control seismic strain accumulation and release. As we move into the next interseismic stage, it is important to assess which preseismic behaviors on the thrust interface remain the same and which change. Will the pre-earthquake pattern of strain accumulation, the locations and timing of slow slip events, and the crustal velocity structure remain unchanged or be modified? Continued geodetic and seismic monitoring are required to address these critical questions.

References

Beroza GC, Ide S (2011) Slow earthquakes and nonvolcanic tremor. *Ann Rev Earth Planet Sci* 39: 271-296.

Feng L, et al. (2012) Active deformation near the Nicoya Peninsula, northwestern Costa Rica, between 1996 and 2010: Interseismic megathrust coupling. *J Geophys Res*

117: doi:10.1029/2012JB009230.

Jiang Y, et al. (2012) Slow slip events in Costa Rica detected by continuous GPS observations, 2002-2011. *Geochem Geophys Geosystems* 13: Q04006.

Malservisi et al. (2015) Multiscale postseismic behavior on a mega-thrust: the 2012 Nicoya earthquake, Costa Rica. *Geochem. Geophys. Geosystems* (In Press).

Outerbridge KC, et al. (2010) A tremor and slip event on the Cocos-Caribbean subduction zone as measured by a global positioning system (GPS) and seismic network on the Nicoya Peninsula, Costa Rica. *J Geophys Res* 115: B10408.

Protti M, et al. (2014) Nicoya earthquake rupture anticipated by GPS measurements of the locked plate interface. *Nature Geosci* 7: 117-121, doi:10.1038/ngeo2038

Schwartz SY, Rokosky, JM (2007) Slow slip events and seismic tremor at circum-Pacific subduction zones. *Rev Geophys* 45: RG3004.

Yue H, et al. (2013) The 5 September 2012 Costa Rica M_w 7.6 earthquake rupture process from joint inversion of high-rate GPS, strong-motion, and teleseismic P wave data and its relationship to adjacent plate boundary interface properties. *J Geophys Res* 118: 5453–5466, doi:10.1002/jgrb.50379.

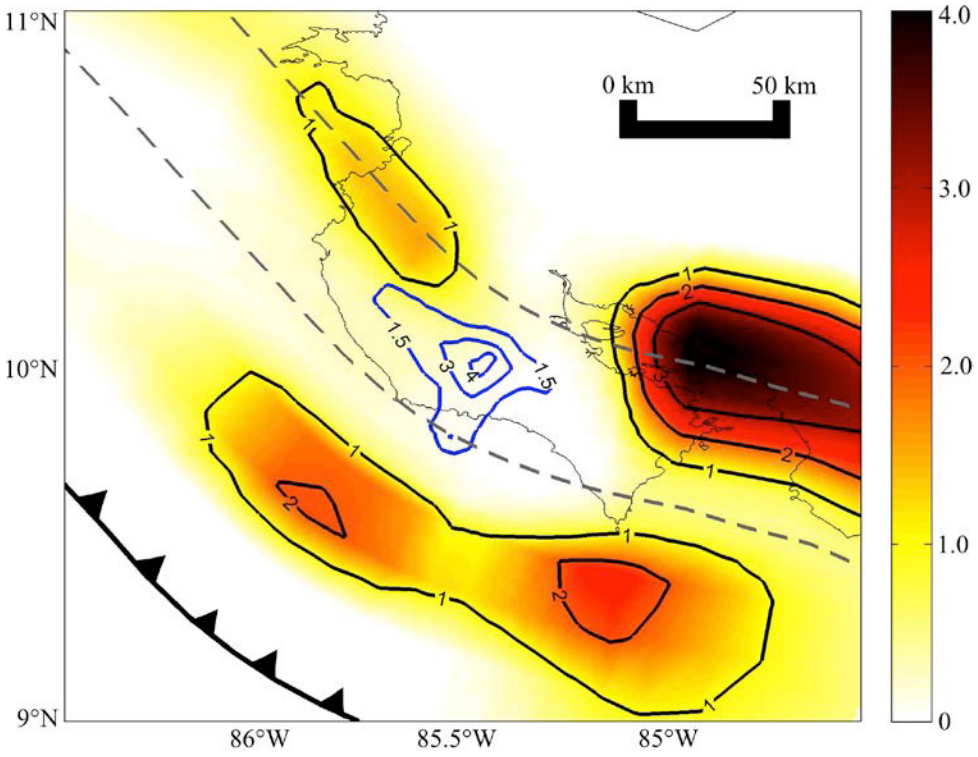

Figure 1. Pre-seismic strain release via slow slip (red and yellow colors, contoured with black lines, labelled in meters of slip) compared to seismic strain release from the 2012 earthquake (blue lines, also contoured in meters of slip). From *Dixon et al.* [2014].

Megathrust Earthquakes and Forearc Uplift Along the Nicoya Peninsula, Costa Rica

Award: 09-48312 (January 2010)

J. Marshall[1], J. Spotila[2]

[1]Cal Poly Pomona University; [2]Virginia Tech University

The Nicoya Peninsula, Costa Rica forms a prominent morphologic high along the Middle America forearc, where the Cocos plate subducts beneath the Caribbean plate at 8.5 cm/yr. This emergent coastal landmass lies directly above the megathrust, along a seismogenic zone that produces frequent major (M≥7.5) earthquakes with an approximate 50-year repeat time (e.g., 1853, 1900, 1950, 2012). The goal of this MARGINS SEIZE research project was to investigate the relationship between upper-plate deformation and seismogenic zone behavior over multiple seismic cycles. Along the Nicoya coast, Quaternary marine and fluvial terraces record net uplift in a pattern that shadows the peninsula's overall topographic form and morphotectonic structure. Terrace mapping, surveying, and age dating (14C, OSL, TCN) reveal uplift variations that coincide with three contrasting domains of subducting seafloor (EPR, CNS-1, CNS-2). Uplift rates vary between 0.1-0.2 m/ky inboard of older EPR crust in the north; 0.2-0.5 m/ky inboard of younger CNS-1 crust along the central coast; and 1.5-2.5 m/ky inboard of CNS-2 seamounts impacting the peninsula's southern tip (Marshall et al., 2012). The most recent major Nicoya earthquakes (1950 M_w7.8; 2012 M_w7.6) generated decimeter-scale coseismic uplift along the central Nicoya coast. The 2012 uplift pattern (Marshall et al., 2013) coincides with the area of pre-event locking (Feng et al., 2012), mainshock slip (Protti et al., 2014), prior 1950 rupture (Guendel, 1986), and 1950 coseismic uplift (Marshall and Anderson, 1995). Most of the 1950 uplift was recovered by gradual interseismic subsidence during six decades of strain accumulation leading to the 2012 rupture. Paleoseismic sediment coring in Nicoya coastal wetlands reveals fragmentary stratigraphic evidence consistent with prior Holocene earthquake induced changes in relative sea level (Spotila et al., 2015). While elastic strain accumulation and release produce short-term cycles of uplift and subsidence, long-term net uplift results in gradual coastal emergence and the growth of topographic relief. Net uplift along the central Nicoya segment may be the product of irrecoverable seismic cycle strain (shortening), coupled with tectonic erosion near the trench and subsequent underplating of eroded material at depth beneath the peninsula. Long-term persistence of the Nicoya seismogenic zone may result from feedback between subduction generated upper-plate thickening and increased coupling along the plate interface due to isostatic loading. Our results are consistent with geophysical observations that indicate along-strike segmentation of the Nicoya seismogenic zone, and the presence of three potential seismic source areas: northern (Papagayo), central (Nicoya), and southern (Cobano). Observed variations in upper-plate uplift along the Nicoya margin may reflect spatial differences in subducting-plate roughness, thermal structure, fluid flow, and seismogenic-zone geometry.

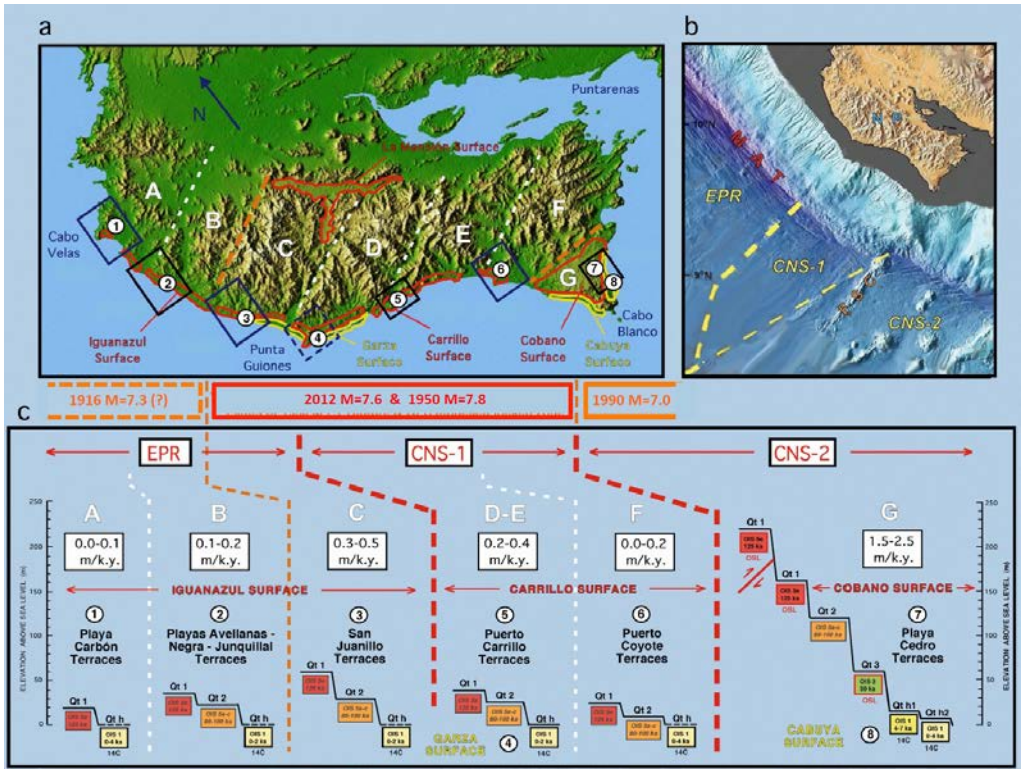

Figure: a) DEM of Nicoya Peninsula (NASA-SRTM) showing uplifted marine and fluvial terraces within late Pleistocene Iguanazul, Carrillo, Cobano, and La Mansion geomorphic surfaces (red areas); and Holocene Garza and Cabuya surfaces (yellow areas). Rectangles outline coastal uplift study areas shown in "c". Dashed white and orange lines mark structural lineaments bounding 8 mountain blocks (A-G) with varying topographic relief. Red and orange rectangles along base of figure show historical earthquake rupture zones. b) DEM of Nicoya margin (NASA-SRTM) linked to offshore bathymetric data (IFM-GEOMAR). Two segment boundaries on the subducting Cocos Plate (Barckhausen et al., 2001) intersect the margin offshore of the Nicoya Peninsula: 1) morphologic break between smooth and rough sea floor domains (thin dashed line); and 2) fracture zone trace (thick dashed line) that divides crust formed at the East Pacific Rise (EPR) from that formed at the Cocos-Nazca spreading center (CNS-1 and CNS-2). c) Schematic of terrace elevations, age data, and uplift rates for numbered study sites (see "a" for locations). Terrace ages based on isotopic dates (14C, OSL, TCN) and sea level curve correlations. Red dashed lines mark EPR, CNS-1, and CNS-2 segment boundaries. Additional dashed lines (white and orange) mark boundaries of blocks A-G. The most rapid uplift affects block G within the 1990 rupture zone inboard of subducting Fisher seamount. Otherwise, rapid uplift affects blocks C-E overlying principal 1950 and 2012 rupture zones. Abrupt decrease in uplift rate to the northwest (between blocks B&C) suggests that the northern end of peninsula may overlie a distinct seismogenic zone segment (possible source of 1916 earthquake).

Marshall, J., Morrish, S., LaFromboise, E., Butcher, A., Ritzinger, B., Wellington, K., Barnhart, A., Kinder, K., Utick, J., Protti, M., Gardner, T., Fisher, D., Simila, G., Spotila, J., Owen, L., Murari, M., Cupper, M., 2012, Morphotectonic segmentation along the Nicoya Peninsula seismic gap, Costa Rica, Central America: *Seismological Research Letters, 83 (2)*, 374.

Marshall, J., Gardner, T., Protti, M., Morrish, M., 2014, The geomorphic footprint of megathrust earthquakes: Morphotectonics of the 2012 Mw7.6 Nicoya Earthquake, Costa Rica, *in* Varga, R. and Markley, M., *eds.*, *Proceedings of the Keck Geology Consortium*, Claremont, California, USA, 11 p.

Spotila, J.A., Marshall, J., DePew, K., Prince, P.S., Kennedy, L., 2015, Potential for geologic records of coseismic uplift and megathrust rupture along the Nicoya Peninsula, Costa Rica: *Journal of Coastal Research, 31 (5)*.

Fluidization in granular materials: the rock record of pressurization and catastrophic loss of strength during deformation

C. D. Rowe and E. E. Brodsky

We studied the role of granular flow during loss of strength in two geological settings: sedimentary fluidization, and rapid fault slip. In both cases, we sought to understand the dynamics governing granular flow, the rheology during flow, and especially the telltale microstructures that might be preserved in the rock record after a dynamic failure in a granular material. Two examples are the extremely thick dolomite gouges of the Naukluft Thrust, Namibia (Figure A and B; Rowe et al. 2012b) and the sedimentary injectites at Panther Beach, California (Figure D; Sherry et al. 2012). In both cases, grain alignment and sorting can be used to make deductions about the style of flow. We also compared injections of gouge to injections of pseudotachylyte – both emanate from fault slip surfaces and are thought to form during earthquakes, and record the coseismic fluid pressure (Rowe et al. 2012a).

Faber, C., Rowe, C. D., Miller, J. A., Fagereng, Å., Neethling, J. H. (2014) Silica gel in a fault slip surface: field evidence for palaeo-earthquakes? Journal of Structural Geology v. 69 108-121

Sherry, T. J., Rowe, C. D., Kirkpatrick, J. D. and Brodsky, E. E. (2012) Dewatering textures in the world's largest exposed injectite complex. Geochemistry Geophysics Geosystems v. 13, n. 1

Rowe, C. D., Kirkpatrick, J. D. and Brodsky, E. E. (2012a) Fault rock injections record paleo-earthquakes. EPSL 335-336 154-166

Rowe, C. D., Fagereng, Å, Miller, J. A. and Mapani, B. (2012b) Signature of coseismic decarbonation in dolomitic fault rocks of the Naukluft Thrust, Namibia. EPSL 333-334 200-210

Rowe, C. D., Backeberg, N., van Rensburg, T., *Maclennan, S., Faber, C., Curtis, C. and Viglietti, P. (2010) Structural geology of Robben Island: Implications for the tectonic environment of Saldanian deformation, South African Journal of Geology 113.1 57-72.

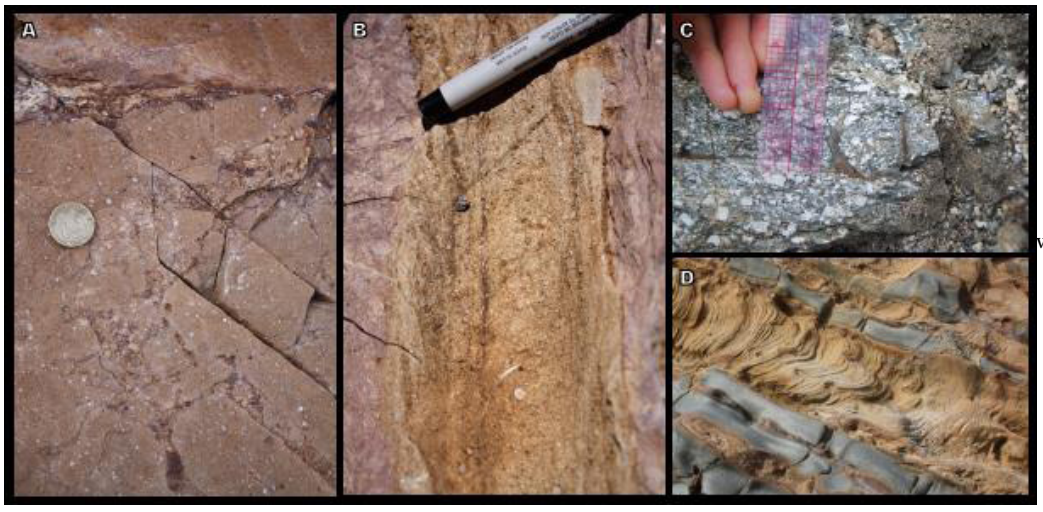

A: Breccias intruding fractures in solidified gouge in the Naukluft Thrust, Namibia (Rowe et al. 2012b). B: Injected dike of dolomite gouge into wallrock of calc-mylonite, Naukluft Thrust, Namibia (Rowe et al. 2012b). Note sorted layers of different grain size gouge parallel to the walls of the dike. C: Injection vein of pseudotachylyte into deformed tonalite wallrock. Aspect ratio corresponds to coseismic fluid pressure in pseudotachylyte melt (Rowe et al. 2012a). D: Three-dimensional fabrics in sand grain orientation within the giant sand injectites, Santa Cruz County, California.